AD-A057 463 TRW DEFENSE AND SPACE SYSTEMS GROUP REDONDO BEACH CALIF F/G 20/1
SAW OSCILLATOR INVESTIGATIONS. CRYSTAL ROTATION, SAW OSCILLATOR--ETC(U)
JAN 78 N66001-77-C-0088
UNCLASSIFIED NL

1 OF 1
AD A057 463

END
DATE FILMED
9-78
DDC

LEVEL II

12

B.S.

SAW OSCILLATOR INVESTIGATIONS

CRYSTAL ROTATION

SAW OSCILLATOR AGING

FINAL REPORT

January 1978

CONTRACT NO. N66001-77-C-0088

Prepared for
NAVAL OCEAN SYSTEMS CENTER
San Diego, California

By

TRW
DEFENSE AND SPACE SYSTEMS GROUP
ONE SPACE PARK • REDONDO BEACH, CALIFORNIA 90278

LEVEL II

12

6

SAW OSCILLATOR INVESTIGATIONS
CRYSTAL ROTATION,
SAW OSCILLATOR AGING.

9 FINAL REPORT. apr 77 - Jan 78.

11 January 1978

12 57 p.

15 CONTRACT NO. N66001-77-C-0088

Prepared for
NAVAL OCEAN SYSTEMS CENTER
San Diego, California

By

TRW
DEFENSE AND SPACE SYSTEMS GROUP
ONE SPACE PARK • REDONDO BEACH, CALIFORNIA 90278

CONTENTS

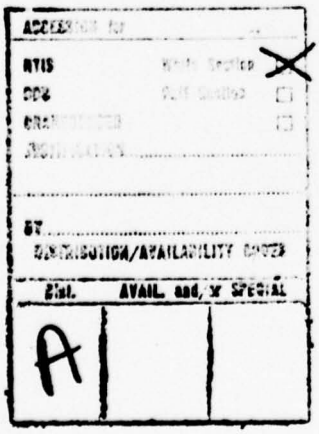

ILLUSTRATIONS

ILLUSTRATIONS (Continued)

TABLES

1. INTRODUCTION AND SUMMARY

This final report describes the results of two surface acoustic wave oscillator studies performed for the Naval Ocean Systems Center under Contract No. N66001-77-C-0088, SAW Oscillator Investigations. The period of performance was April 1977 through January 1978. The first study demonstrated a new ~~TRW-devised~~ technique for varying the frequency of operation of SAW delay lines. The second study continued the ongoing aging test of four 250 MHz oscillators which was started in July 1975, and measured the aging rate of a new pair of oscillators fabricated using SAW delay lines with chrome/gold metallization.

Future high performance communication systems will require frequency sources at UHF and microwave frequencies. SAW oscillators offer several advantages over bulk cyrstal oscillator multiplier chain type sources. The higher fundamental frequency capability of the SAW device eliminates the need for a multiplier chain, thus reducing size, weight, and power while providing superior phase noise characteristics.

One fundamental disadvantage of SAW oscillators is that for each new frequency of operation required, a new photomask for the SAW delay line must be designed and fabricated. The purpose of the contractual work was to investigate a technique for fabricating SAW delay lines with different center frequencies using a single common photomask. The key to this development is the rotation of the photomask with respect to the X-axis of the ST-cut quartz SAW substrate.

Until this time, the center frequency of a SAW delay line was determined by the physical dimensions of the transducer pattern and by the acoustic propagation velocity (v_a) of the piezoelectric material. Since v_a is a property of the delay line material, v_a is not readily adjusted. The physical dimensions of the transducer could previously be adjusted only by having a new SAW photomask made, a process costing $2000 to $3000 per iteration. Further, even though mask makers are able to hold the extremely tight tolerance of ±0.01 micron, that tolerance leads to a frequency error of ±2 MHz at 500 MHz. Since delay line bandwidths are typically only ±250 kHz at 500 MHz, the SAW oscillator cannot be tuned to compensate for the mask tolerances. Thus, the only choice when exact frequency setability is required has been to pay for several mask iterations. This is not a serious problem if a large quantity of SAW oscillators at the same frequency are required, but is expensive when the quantities are small.

TRW has demonstrated that by changing the orientation of the transducer pattern relative to the crystal axis on which the transducer is fabricated, it is possible to make minor adjustments of the delay line frequency. This technique promises to eliminate costly photomask iterations for minor frequency adjustments.

The procedure followed to evaluate this effect was to fabricate the same transducer pattern on ST-cut quartz for several rotation angles. A total of 14 SAW delay lines was

fabricated; two each at rotation angles of 0, 15, 30, 45, 60, 75, and 90 degrees. The center frequency, insertion loss, and temperature coefficient were measured for each of these delay lines.

This report documents the fabrication and test of the rotated SAW delay lines. Complete data of the center frequency, insertion loss, and temperature coefficient as a function of rotation angle is presented. The results of the program demonstrated that the technique was useful for varying the basic frequency resulting from a single photomask over a 10% range. This is more than sufficient for compensating for mask fabrication uncertainties.

Another major problem limiting the use of surface acoustic wave oscillators as frequency sources in high performance applications is that their long-term frequency drift or aging is considerably greater than conventional bulk crystal oscillators. The long-term aging rate of the best SAW oscillators is approximately 100 times greater than the aging rate of high quality bulk crystal oscillators. The nature of the SAW delay line aging mechanism has not been identified but likely sources include factors such as stress relaxation within the crystal and the metallized finger pattern, and contamination of the crystal surface by foreign material.

To date, a total of over 10 oscillator-years of aging data has been accumulated as part of this program. Four 250 MHz oscillators have been on continuous life test for the past 2-1/2 years. When maintained in a stable environment, these oscillators have a demonstrated aging rate of -5 ppm per year.

As a part of this study, two SAW oscillator aging experiments were designed and conducted. The experiments were aimed at investigating two aspects of the SAW aging problem: the effects of temperature cycling, and changing the metallization scheme from chrome-aluminum to chrome-gold. A temperature cycling test was conducted to determine both the magnitude of cycle-induced aging rate changes and the degree of similarity between aging rates of the four SAW oscillators. As a result of stressing the oscillators in this fashion, the aging rate increased from under -5 ppm per year to over -26 ppm per year.

The second aging experiment entailed the fabrication and life testing of two SAW oscillators using chrome-gold metallized delay lines. This experiment was designed to investigate the relationship between the SAW delay line metallization and its aging rate. Chrome-gold metallization was chosen since it is used for contacts on high quality bulk crystals. During the first 3 months of aging, these oscillators have demonstrated an aging rate of approximately twice that of the chrome/aluminum oscillators during their first 3 months. Extended aging of these oscillators will be necessary to confirm these test results.

This program has been particularly important because it has recorded the long-term aging rates of a set of four SAW oscillators over a 2-1/2 year period. These oscillators have been subjected to a wide variety of controlled environments and the resulting aging rates recorded. It has been demonstrated that if the true aging rate of a SAW oscillator is to be determined, it is not sufficient to test the oscillator in a carefully stabilized environment, but rather one which more closely simulates actual operating conditions.

2. ROTATED SAW DELAY LINE FABRICATION

A total of 14 rotated SAW delay lines was fabricated for these experiments on ST-cut quartz using standard photolithographic techniques. The dependence of key delay line parameters (velocity, coupling coefficient, temperature coefficient) was calculated as a function of rotation angle. The calculated values were found to be in good agreement with the measured data for the full 90° range of rotation.

2.1 SAW DEVICE MATERIAL

ST-cut quartz, which was the SAW substrate material used for the crystal rotation experiments, has found widespread use in SAW device applications because of its excellent temperature stability. ST-cut quartz is cut at an angle of 42.75° from the Y-axis. On ST-cut quartz, the surface acoustic wave is normally propagated along the X-axis. This is illustrated in Figure 2-1. Because quartz is an anisotropic crystal, its velocity, piezoelectric coupling coefficient, and temperature coefficient are functions of the surface acoustic wave propagation direction.[1] Figure 2-2 shows the calculated dependence of the surface wave velocity as a function of propagation direction on ST-cut quartz. The surface acoustic wave velocity increases as the direction of propagation is rotated from the X-direction, reaching a maximum at 90°.

The calculated electromechanical coupling coefficient (k^2) for surface acoustic waves on ST-cut quartz is also a function of propagation direction as shown in Figure 2-3. The electromechanical coupling coefficient is calculated from $k^2 = 2\ (\Delta v/v)$, where $\Delta v/v$ is the fractional change in the surface acoustic wave velocity when the substrate surface is metallized. The electromechanical coupling coefficient first increases as one rotates from the X-axis and then decreases to zero at 90° from the X-axis. Thus, no surface acoustic wave can be generated at 90° from the X-axis. The calculated first order temperature coefficient of delay as a function of propagation direction is shown in Figure 2-4. This coefficient is zero for propagation directions of 0, 37, 143, and 180 degrees.

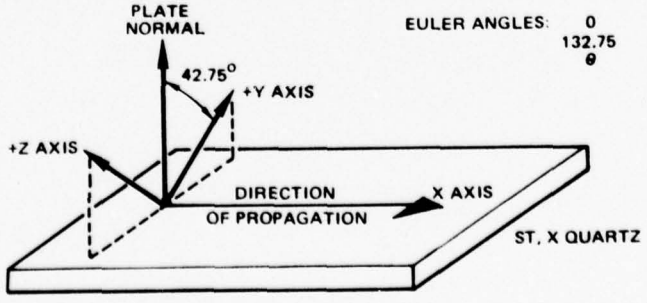

Figure 2-1. ST-CUT Quartz

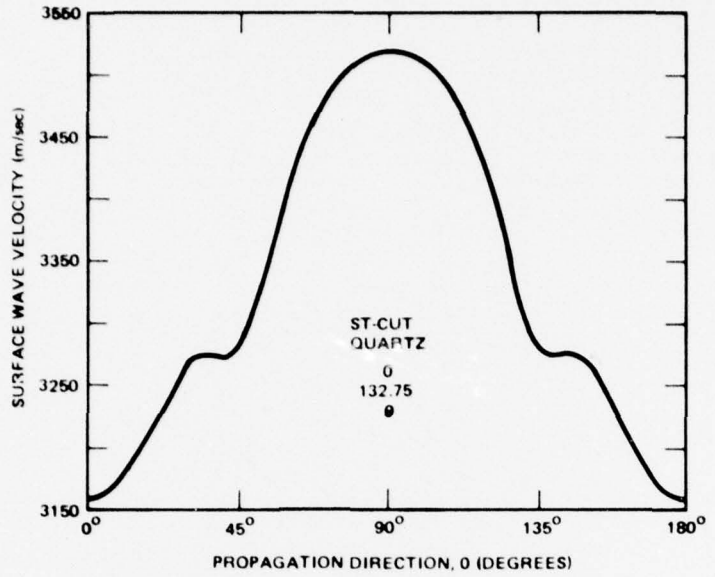

Figure 2-2. Calculated Surface Acoustic Wave Velocity vs Propagation Direction for ST-Cut Quartz

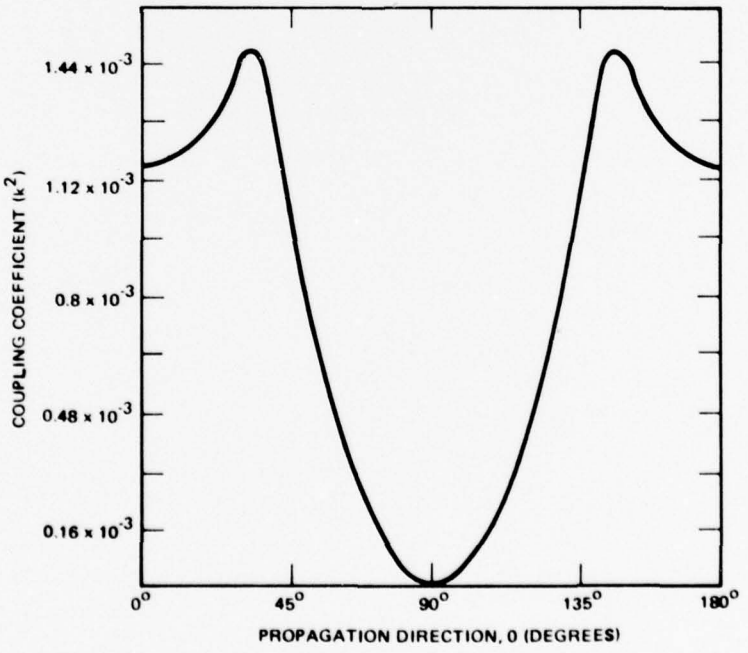

Figure 2-3. Calculated Electromechanical Coupling Coefficient vs Propagation Direction for ST-Cut Quartz

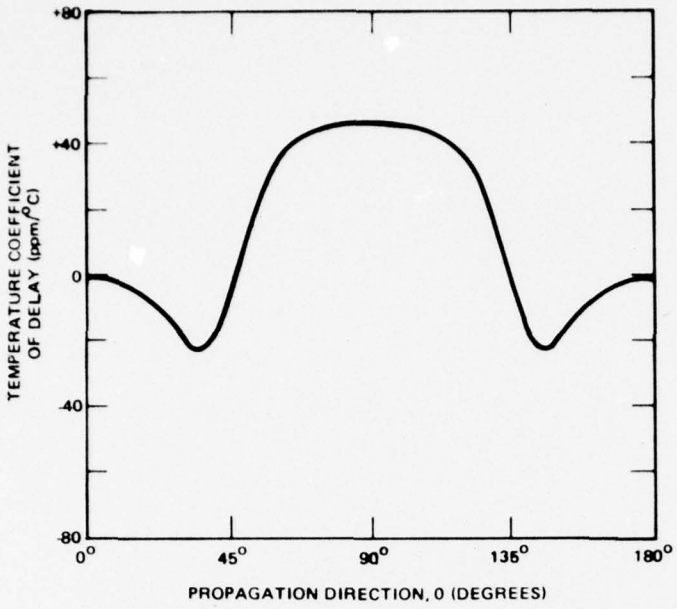

Figure 2-4. Calculated Temperature Coefficient of Delay vs Propagation Direction for ST-Cut Quartz

2.2 SAW TRANSDUCER DESIGN

The SAW delay lines fabricated for this program were of the closed structure configuration as shown in Figure 2-5. One transducer has a total of 149 fingers and the other has 213 fingers. The center-to-center separation is 106 λ, where λ is the SAW wavelength. When the delay lines were fabricated on ST-cut quartz along the X-axis (0° rotation), the center frequency of operation was 250 MHz.

The equivalent circuit approach was used to calculate the characteristic impedance and the minimum insertion loss of the transducer in the passband. The "cross-field" equivalent circuit model was used since there were many fingers in the transducers. The equivalent circuit of the input admittance of the interdigital transducer is represented by a radiation conductance in parallel with the transducer radiation susceptance and static capacitance. This equivalent circuit is illustrated in Figure 2-6.

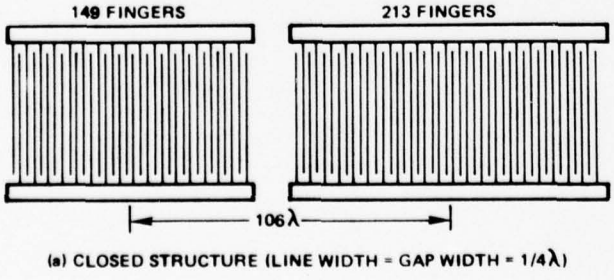

Figure 2-5. Basic SAW Delay Line Configuration

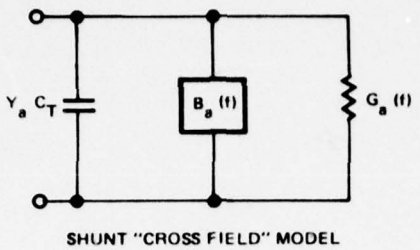

SHUNT "CROSS FIELD" MODEL

Figure 2-6. Shunt Representation for Electrical Input Admittance

The radiation conductance is given as

$$G_a(f) = G_{T_o}\left(\frac{\sin x}{x}\right)^2 \qquad (1)$$

where

$x = N\pi\ (f - f_o)/f_o$

$G_o = \delta k^2 N^2\ C_T f_o$

N_2 = number of finger pairs of the transducer

k^2 = the piezoelectric coupling constant of the substrate

$C_T = NC_S W$

C_S = capacitance per finger pair

W = the aperture of the transducer

The radiation susceptance can be obtained from the Hilbert transform of the radiation conductance. At the transducer synchronous frequency ω_o

$$B_a\ (\omega_o) = 0$$

The conversion efficiency of a transducer can be calculated using its equivalent circuit which is a radiation conductance in parallel with the radiation susceptance and total static capacitance. The acoustic wave power is equal to the amount of electrical power delivered to the radiation conductance $G_a(\omega)$. Solving for the power delivered to G_a compared to the maximum power available from a generator of conductance G_L and allowing for the bidirectional loss of the transducer gives

$$p = \frac{2\ G_L\ G_a(\omega)}{(G_L + G_a(\omega))^2 + (2\pi f_o C_T + B_a(\omega))^2} \qquad (2)$$

Thus, utilizing the cross-field equivalent circuit model, the input admittance or impedance of the transducer and the delay line insertion loss can be easily calculated.

2.3 FABRICATION TECHNIQUES

Standard photolithographic techniques were used to fabricate the surface acoustic wave delay lines, although special precautions were taken to ensure good replication of the transducers. The original mask for the 250 MHz SAW delay line was fabricated on a standard 60-mil thick glass plate coated with anti-reflecting chrome. This photomask was then transferred to a conformal flexible photomask of 7-mil thickness. The use of a flexible photomask minimized diffraction effects which occur during the ultraviolet exposure of the photoresist, thus ensuring good linewidth resolution for the transducers.

All of the rotated SAW delay lines were fabricated using an etching process. A thin metal film was first deposited on the substrate by flash evaporating about 100 Å of chromium followed by an evaporated film of 1000 Å of aluminum. The chromium was used to ensure good adhension of the aluminum film. Both films were evaporated at a low substrate temperature to minimize the grain size.

The transducer patterns were transferred onto the metal film using a light field mask and Shipley 1350 positive photoresist. The photoresist was then exposed and developed to form a mask over the metal film. A vacuum frame with a thin rubber membrane was used to lift the quartz substrate into intimate contact with the photomask to improve the line width resolution. Finally, the pattern was defined by chemically etching away the undesired metal.

2.4 PROPAGATION ANGLE MEASUREMENTS

The ST-cut quartz substrates used for this program were purchased from Sawyer Research Products. These crystals were X-ray oriented by the vendor and the long edges of the crystal blanks cut parallel to the X-axis to within $\pm 0.5^{o}$.

The quartz substrates were mounted on a 4-inch circular plate which had calibration angles around its circumference. The circular plate was then mounted on the diamond saw holder for slicing out the individual SAW substrates. By a micromanipulator adjustment, the large quartz crystal was then oriented for cutting to within $\pm 0.5^{o}$ of the desired propogation directions (0, 15, 30, 45, 60, 75, and 90 degrees). The delay lines were then fabricated with the direction of propagation parallel to the long edge of the quartz substrates. It is estimated that the propogation direction is accurate to within $\pm 1^{o}$ of the desired rotation angle.

Individual quartz substrates were selectively sampled to confirm the orientation. To do this, they were mounted into a goniometer and X-rayed along the X-axis. Figure 2-7 shows the Laue X-ray diffraction pattern resulting from an ST-cut quartz substrate oriented at 0^{o} from the X-axis

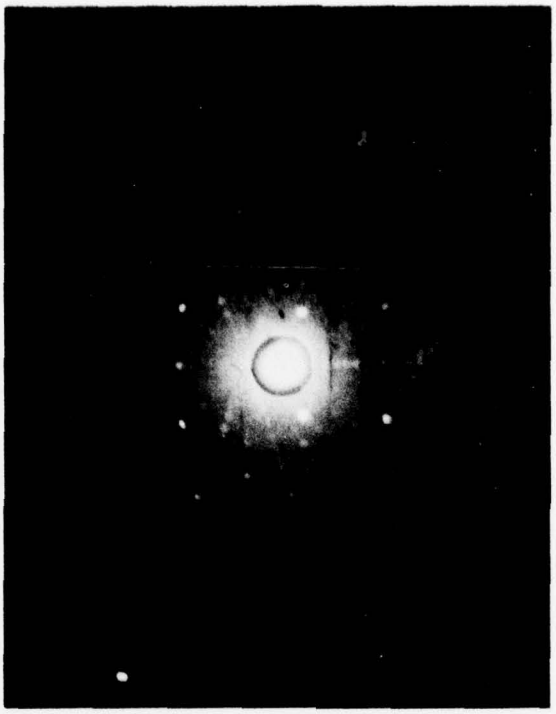

Figure 2-7. Laue Pattern of ST-Cut Quartz in Approximately the X-Axis Orientation

2.5 CRYSTAL ROTATION MEASUREMENTS

Section 2.1 showed the surface acoustic wave velocity, electromechanical coupling coefficient, and the temperature coefficient of delay to be functions of the surface acoustic wave propagation direction. To verify this, 18 SAW delay lines were fabricated with identical transducer patterns at various directions on ST-quartz. They were fabricated in pairs at rotated angles of 0, 15, 30, 45, 60, 75, 80, 85, and 90 degrees, with respect to the X-axis.

The surface acoustic wave or Rayleigh wave is a nondispersive wave; thus, the velocity of propagation is directly proportional to the center frequency of operation of the SAW delay line. Figure 2-8 shows the calculated and measured center frequency of operation. For the calculated solid curve, the free surface wave velocity shown in Figure 2-2 was used. Because of the strong second order effect caused by the interdigital transducer and beam steering effects, the passband response of the delay lines was distorted and skewed. Thus, the center frequency of the delay lines was determined by measuring the first frequency null on either side of the passband. Figure 2-8 clearly shows there is excellent agreement between theory and experiment.

The equivalent circuit equations discussed in Section 2.2 were used to calculate the transducer input admittance for the various propagation directions. The results of these calculations are tabulated in Table 2-1. From these admittance values and the electromechanical coupling coefficient of ST-cut quartz shown in Figure 2-3, the

Table 2-1. Calculated Transducer Input Admittance as a Function of Propagation Direction

Propagation Direction	Transducer A (149 Fingers; C_T = 9.25 pF)		Transducer B (213 Fingers; C_T = 13.25 pF)	
	G (mmhos)	B_C (mmhos)	G (mmhos)	B_C (mmhos)
0^o	1.59	14.52	3.26	20.8
15^o	1.69	14.70	3.47	21.05
30^o	2.07	15.04	4.25	21.54
45^o	1.48	15.09	3.04	21.62
60^o	0.65	15.72	1.34	22.51
75^o	0.182	16.10	0.37	23.06
80^o	0.091	16.16	0.19	23.15
85^o	0.031	16.19	0.063	23.20
90^o	0	16.21	0	23.21

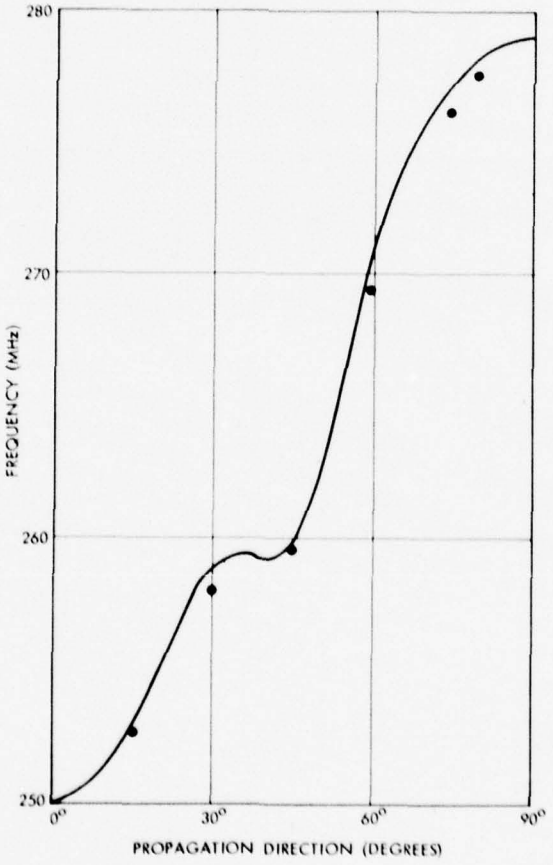

Figure 2-8. Measured vs Calculated SAW Delay Line Center Frequency as a Function of Rotation Angle

insertion loss of the SAW delay lines was calculated using equation (2). Because of the small propagation length (106 wavelengths), the propagation loss and beam steering loss were neglected. The results of the calculation are indicated by the solid curve in Figure 2-9, together with the measured data. The discrepancy between calculated and measured values is attributed to partial transducer matching (due to bond wires) and electrical feedthrough between input and output transducers.

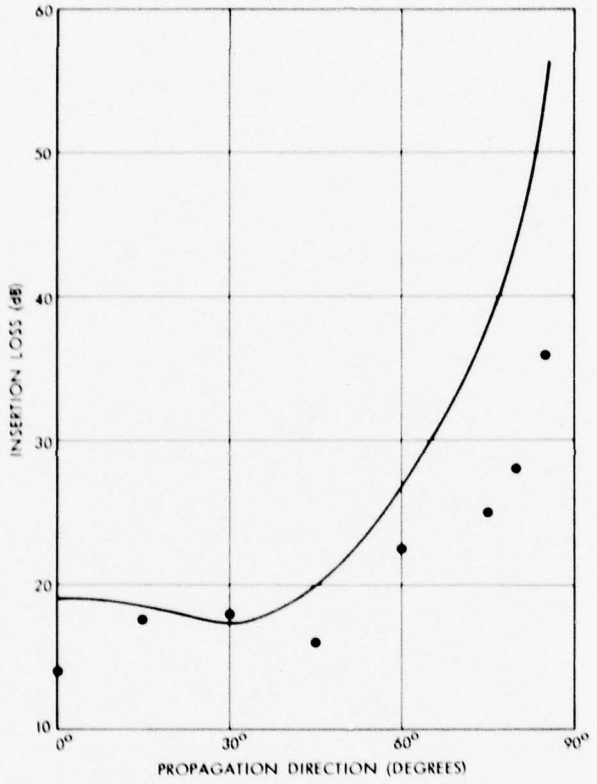

Figure 2-9. Measured vs Calculated SAW Delay Line Insertion Loss as a Function of Rotation Angle

The electromechanical coupling coefficient goes to zero at 90^{0} from the X-axis; thus there is no surface wave excited in that direction. However, a shallow bulk acoustic wave (SBAW) which was discovered at TRW can be excited. This SBAW is a fast shear wave which propagates close to the surface of the substrate. [2,3] The frequency of operation is about 1.6 times higher than that of X-propagated SAW's. The insertion loss is comparable to that of SAW devices.

2.6 CONCLUSION

The experimental results of the rotation measurement verify existing predictions. Physical parameters, including surface acoustic wave velocity, electromechanical coupling coefficient, and the temperature coefficient of delay, were calculated and tabulated using bulk acoustic wave data. Our rotation measurements show that the center frequency of a transducer can be predicted using this surface acoustic wave velocity. For a given linewidth of a transducer, one can calculate the center frequency of response as a function of rotation angle from the surface acoustic wave velocity shown in Figure 2-2. For the experiments, this free surface velocity can be used since the second effects are negligible. Both the piezoelectric loading and mass loading of the fingers were small. The piezoelectric loading was small because the piezoelectric coupling coefficient for ST-cut quartz is small. The mass loading was small because the metallization was only 100 Å of chromium overlaid with 1000 Å aluminum, and the operating frequency was between 250 and 280 MHz. Thus, even using free surface velocities as shown in Figure 2-2, the calculated center frequencies were close to the measured values as shown in Figure 2-8.

The values of the electromechanical coupling coefficient together with the cross-field equivalent circuit model were used to calculate the transducer characteristic impedance and conversion loss as a function of rotation angle. In these calculations, the static capacitance was assumed to be a constant and to be independent of rotation angle. Table 2-1 lists the input admittance of the transducer used in these measurements. From these values, one can calculate the insertion loss of the SAW delay lines. These results are shown in Figure 2-9 along with the measured values. The difference between calculated and measured values is attributed to partial transducer matching and electrical feedthrough.

Thus, using physical parameters determined by bulk acoustic wave data, one can predict the behavior of the surface acoustic wave as a function of rotation angle. However, the transducer center frequency shows better agreement to the calculations than the insertion loss.

REFERENCES

1. A. J. Slobodnik, Jr., "The Temperature Coefficients of Acoustic Surface Wave Velocity and Delay on Lithium Tantalate, Quartz, and Tellurium Dioxide," AFCRL-72-0082.

2. K. H. Yen, K. L. Wang, and R. S. Kaqiwada, "Efficient Bulk Wave Excitation on ST Quartz," Electronic Letters, 13, 37 (1977).

3. K. H. Yen, K. L. Wang, R. S. Kagiwada, and K. F. Lau, "Interdigital Transducers--A Means of Efficient Bulk Wave Excitation," 31st Annual Frequency Symposium.

3. ROTATED SAW DELAY LINE CHARACTERIZATION

The 14 rotated SAW delay lines (two each at rotation angles of 0, 15, 30, 45, 60, 75, and 90 degrees) were carefully characterized to determine the relationship between rotation angle and performance. The parameters which were monitored were center frequency, insertion loss, bandwidth (Q), passband shape, and temperature coefficient. The results of this test program indicate that there are two different modes of operation. The first is the normal surface acoustic wave mode, and was the dominant mode for the 0^{o} through 75^{o} rotation angles. The second is a shallow bulk mode and was the dominant mode for the 90^{o} rotation angle. To further evaluate the two different modes, additional delay lines with rotation angles of 80^{o} and 85^{o} were fabricated. Both of these delay lines also operated in the shallow bulk mode. This result indicates that the transition between dominant mode occurs between 75^{o} and 80^{o}.

3.1 TEST PROCEDURE

To ensure the validity of the program results, a test plan for evaluating the rotated delay lines was developed. This test procedure was than followed for each delay line. The tests were done on a swept frequency basis and included passband, center frequency, insertion loss, and return loss. They were performed on a semi-automatic basis using an HP8505 network analyzer.

Following the swept frequency tests, each delay line was assembled into a test oscillator circuit to determine its temperature stability. One common set of loop electronics was used for all of the tests to eliminate the potential uncertainty associated with using a different electronics with each oscillator. The output frequency for each oscillator was then measured over the $-50^{o}F$ to $+150^{o}F$ temperature range.

3.2 TEST RESULTS

This section presents the raw data from the characterization and summarizes the relationship between each major parameter and rotation angle. The results are summarized in Table 3-1.

3.2.1 Frequency as a Function of Rotation

The prime motivation for this task was to demonstrate that the frequency of operation of a SAW delay line could be varied by rotating the direction of acoustic wave proagation with respect to the X-axis of the ST-cut quartz substrate. To document this effect, 14 SAW delay lines were fabricated, two each at rotation angles of 0, 15, 30, 45, 60, 75, and 90 degrees. In addition, four more delay lines were fabricated at angles of 80^{o} and 85^{o} to provide further data for the shallow bulk mode of operation.

Table 3-1. SAW Delay Line Characterization Summary

ROTATION ANGLE	IDENTIFICATION	PASSBAND CENTER FREQUENCY MHz	INSERTION LOSS dB	Q	3 dB BANDWIDTH		TEMPERATURE STABILITY -50°F TO +150°F		FIRST ORDER TC PPM/°C
					PERCENT	Mhz	SHAPE	PERCENT	
0°	A	249.150	13.5	357	0.28	0.700	PARABOLIC	±0.006	0
	B	249.200	13.5	333	0.30	0.750	PARABOLIC	±0.006	0
15°	A	252.350	15.5	333	0.30	0.750	PARABOLIC	±0.008	+1.3
	B	252.550	16.5	312	0.32	0.800	PARABOLIC	±0.006	+0.8
30°	A	258.600	16.0	117	0.85	2.200	POSITIVE/LINEAR	±0.070	+12.6
	B	258.550	14.5	138	0.72	1.850	POSITIVE/LINEAR	±0.070	+12.6
45°	A	258.100	15.5	100	1.00	2.580	POSITIVE/LINEAR	±0.038	+ 6.8
	B	258.500	16.0	105	0.95	2.450	POSITIVE/LINEAR	±0.038	+ 6.8
60°	A	268.100	20.0	714	0.14	0.375	NEGATIVE/LINEAR	±0.170	-30.6
	B	268.500	26.0	714	0.14	0.375	NEGATIVE/LINEAR	±0.160	-28.8
75°	A	276.900	27.0	909	0.11	0.300	NEGATIVE/LINEAR	±0.220	-39.6
	B	276.900	26.5	714	0.14	0.380	NEGATIVE/LINEAR	±0.210	-37.8
80°	A	371.300	22.0	217	0.46	1.700			
	B	370.000	24.0	243	0.41	1.500	-		
85°	A	385.700	21.5	277	0.36	1.400			
	B	387.100	18.5	322	0.31	1.200			
90°	A	393.800	15.0	400	0.25	1.000	POSITIVE/LINEAR	±0.140	+27.7
	B	393.900	13.5	357	0.28	1.100	POSITIVE/LINEAR	±0.150	+30.5

The results of this investigation indicated that there were two different modes of operation for the rotated delay lines. The first mode, which is the normal surface acoustic wave, existed for rotation angles of 0^{o} through 75^{o}. Over this 75^{o} range, the delay line center frequency shifted from 249.200 to 276.900 MHz, an increase of 11 percent. The frequency as a function of rotation angle is shown in Figure 3-1.

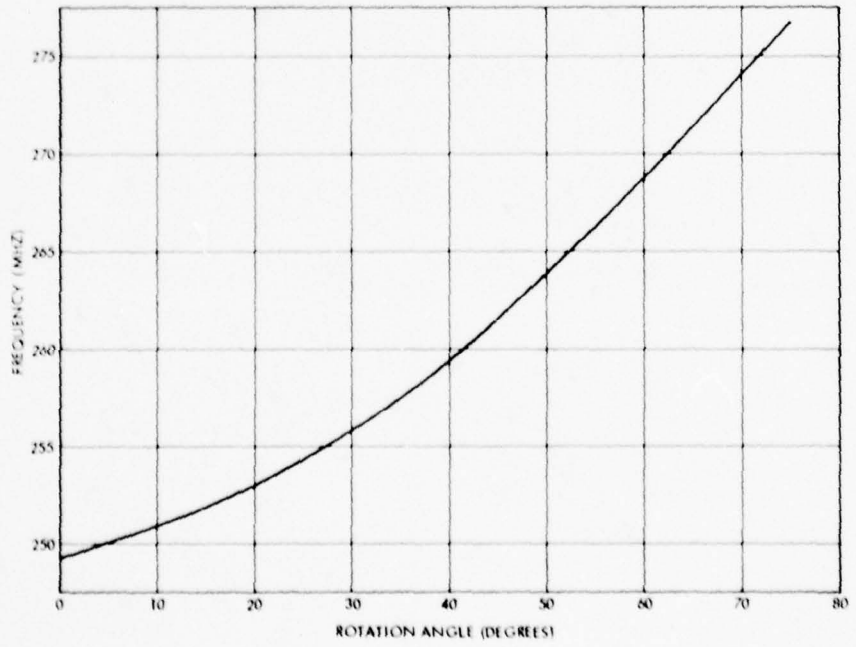

Figure 3-1. SAW Delay Line Frequency as a Function of Rotation Angle

The second mode of operation is a shallow bulk wave. This mode propagates for rotation angles between 80^{o} and 90^{o}. Over this 10^{o} range, the frequency of operation varied between 370.000 and 393.900 MHz, for a total shift of 6.3 percent. The data is shown in Figure 3-2.

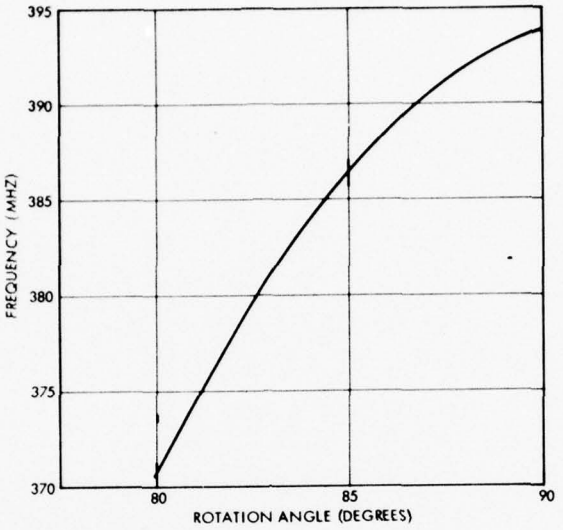

Figure 3-2. Frequency of Operation vs Rotation/Angle for Shallow Bulk Mode

These tests demonstrated that the use of crystal rotation is a viable technique of controlling the center frequency of SAW delay lines. For a 15^{o} rotation from 0^{o}, the frequency variation was 8.7×10^{-4}/degree. A tolerance of $\pm 0.50^{o}$ can be held during alignment of the SAW mask and crystal. This translates to an accuracy of $\pm$100 kHz at 250 MHz which is compatible with the remaining fabrication tolerances.

3.2.2 Passband Distortion

The swept response of each of the SAW delay lines was recorded to determine the passband characteristics as a function of rotation angle. The swept responses are shown in Figures 3-3 through 3-16. From these graphs, it is evident that the passband becomes increasingly distorted as the rotation angle is increased beyond 45^{o}. Two parameters which were measured to analyze this distortion were unmatched insertion loss and Q (f_o/3 dB BW), both of which are plotted as a function of rotation angle in Figures 3-17 and 3-18.

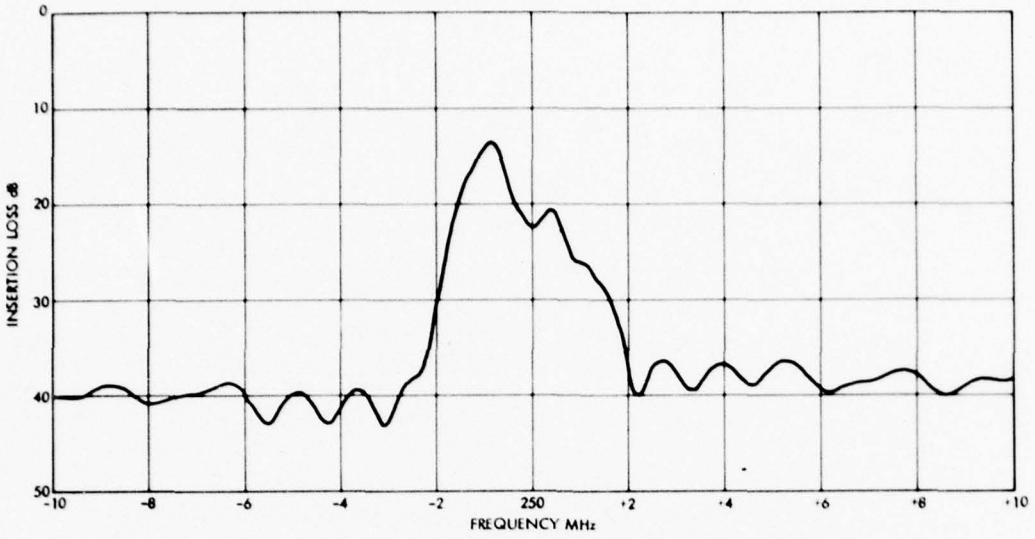

Figure 3-3. 0 Degree "A" Rotated SAW Delay Line
Passband Characteristic

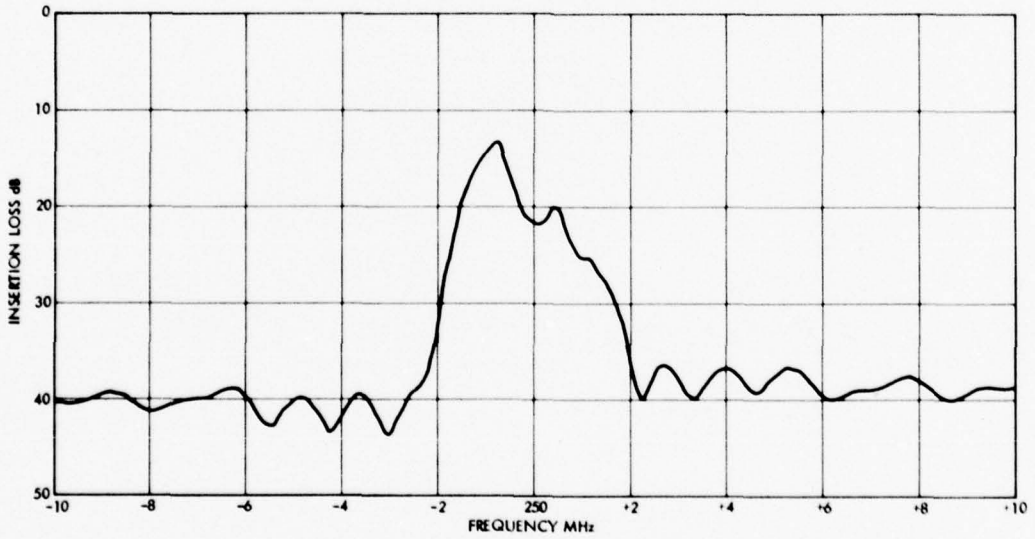

Figure 3-4. 0 Degree "B" Rotated SAW Delay Line
Passband Characteristic

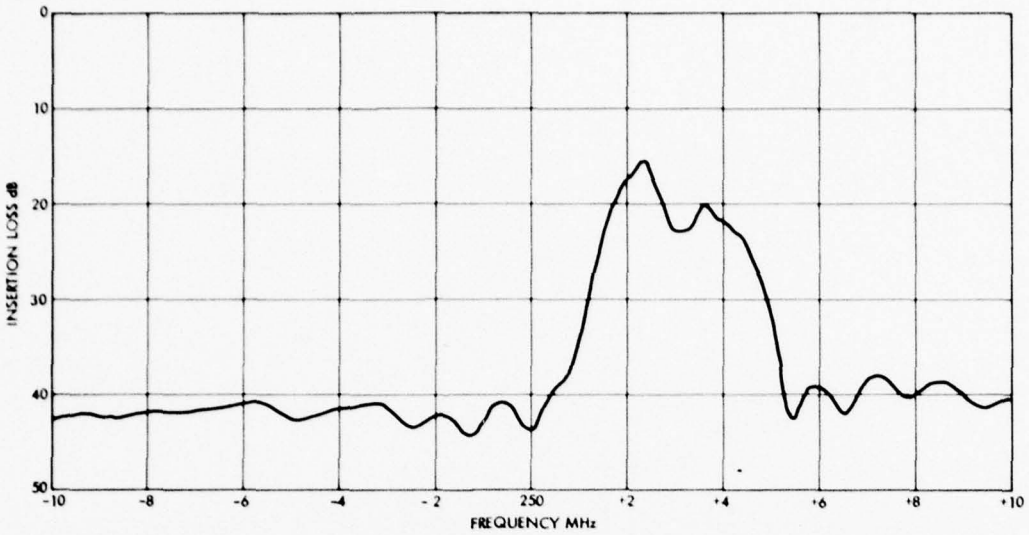

Figure 3-5. 15 Degrees "A" Rotated SAW Delay Line Passband Characteristic

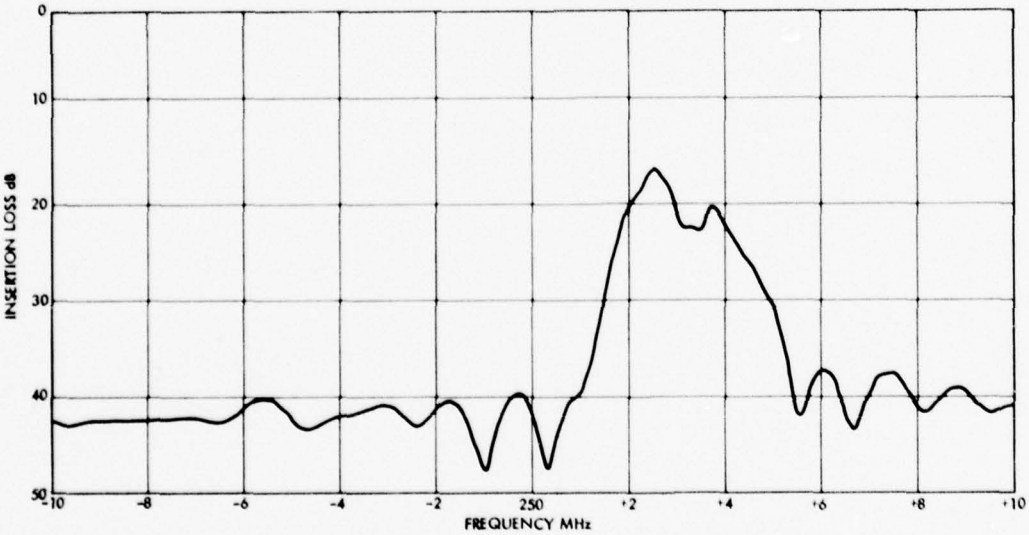

Figure 3-6. 15 Degrees "B" Rotated SAW Delay Line Passband Characteristic

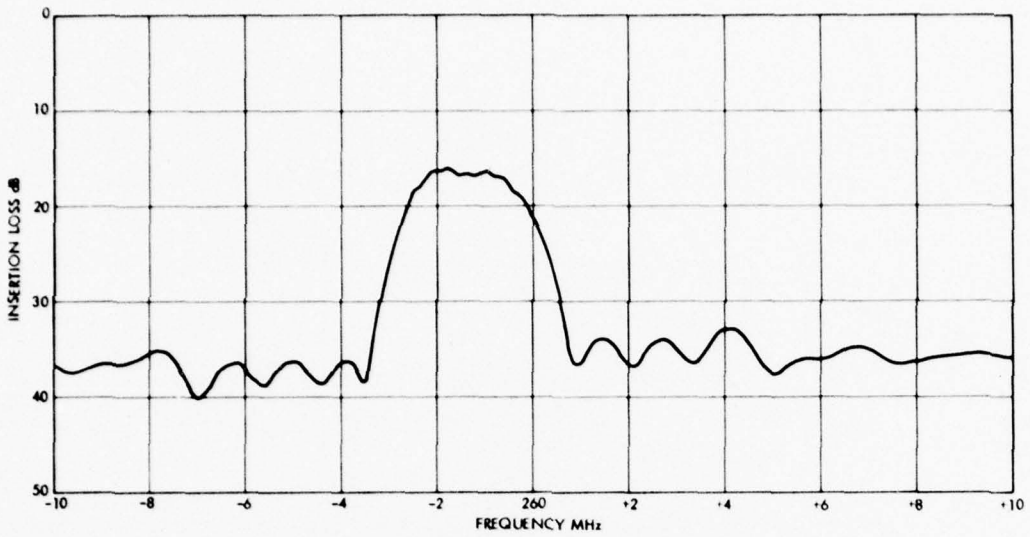

Figure 3-7. 30 Degrees "A" Rotated SAW Delay Line Passband Characteristic

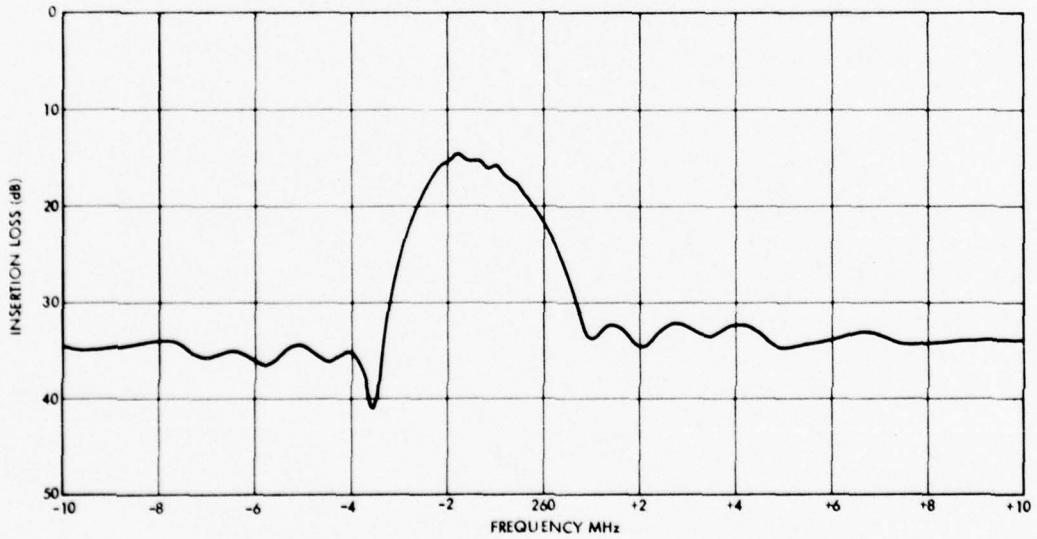

Figure 3-8. 30 Degrees "B" Rotated SAW Delay Line Passband Characteristic

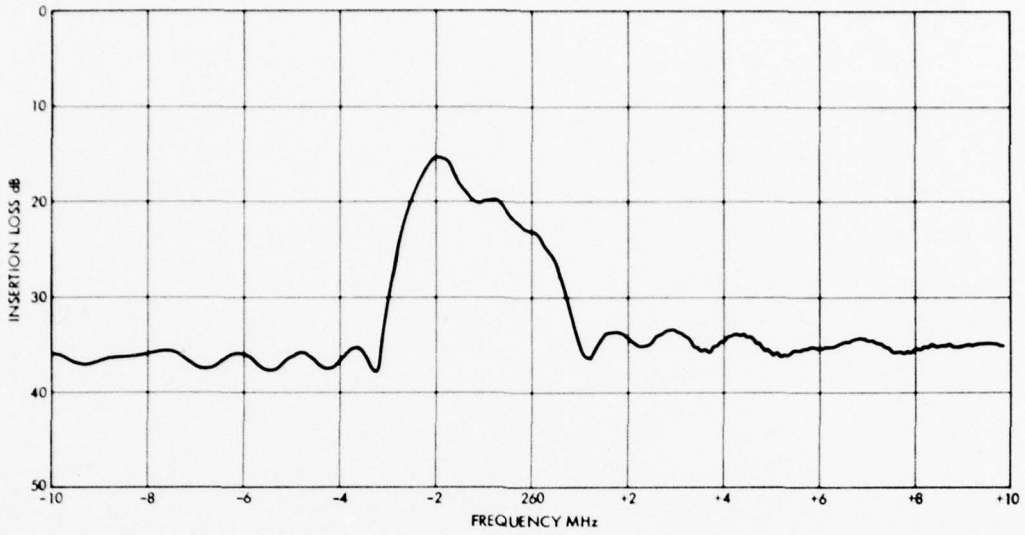

Figure 3-9. 45 Degrees "A" Rotated SAW Delay Line Passband Characteristic

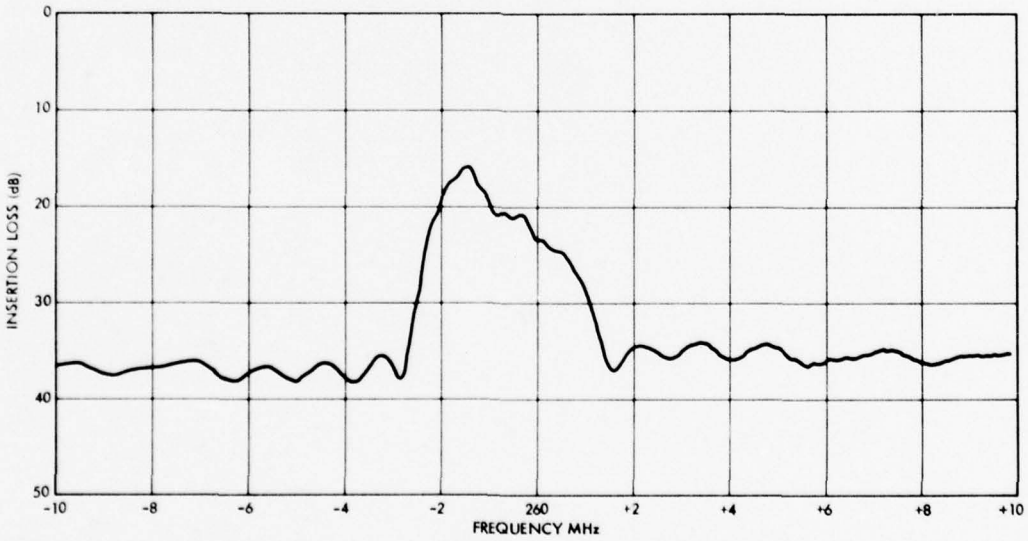

Figure 3-10. 45 Degrees "B" Rotated SAW Delay Line Passband Characteristic

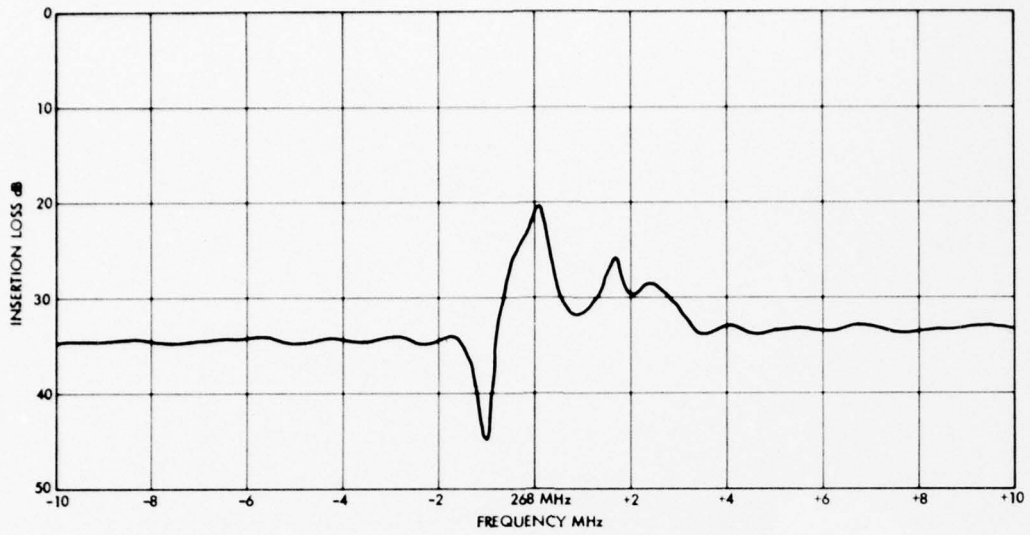

Figure 3-11. 60 Degrees "A" Rotated SAW Delay Line Passband Characteristic

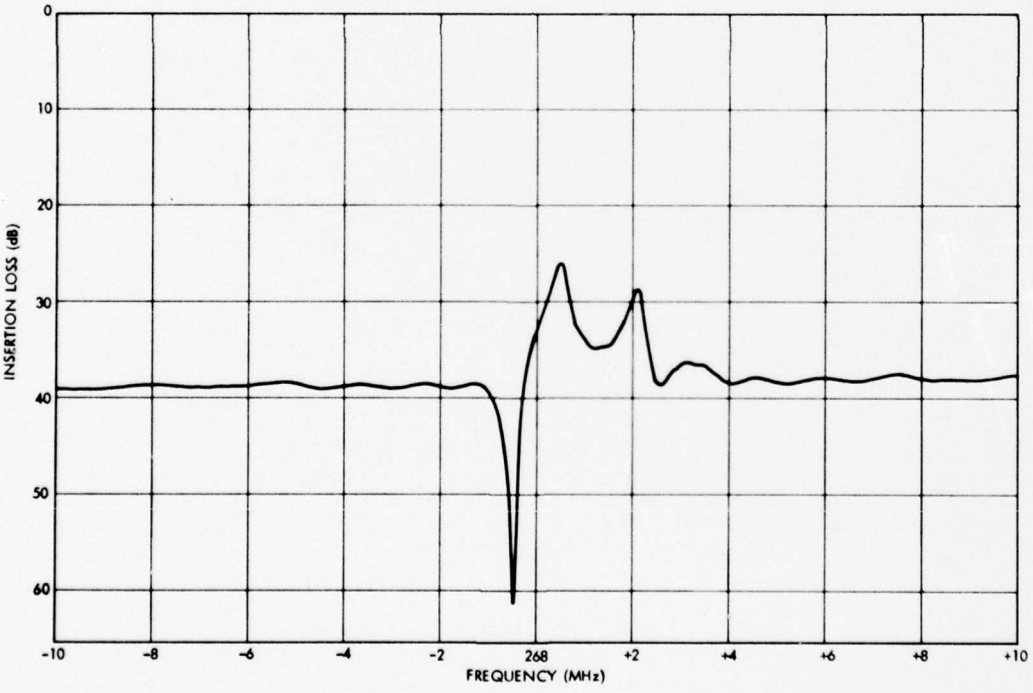

Figure 3-12. 60 Degrees "B" Rotated SAW Delay Line Passband Characteristic

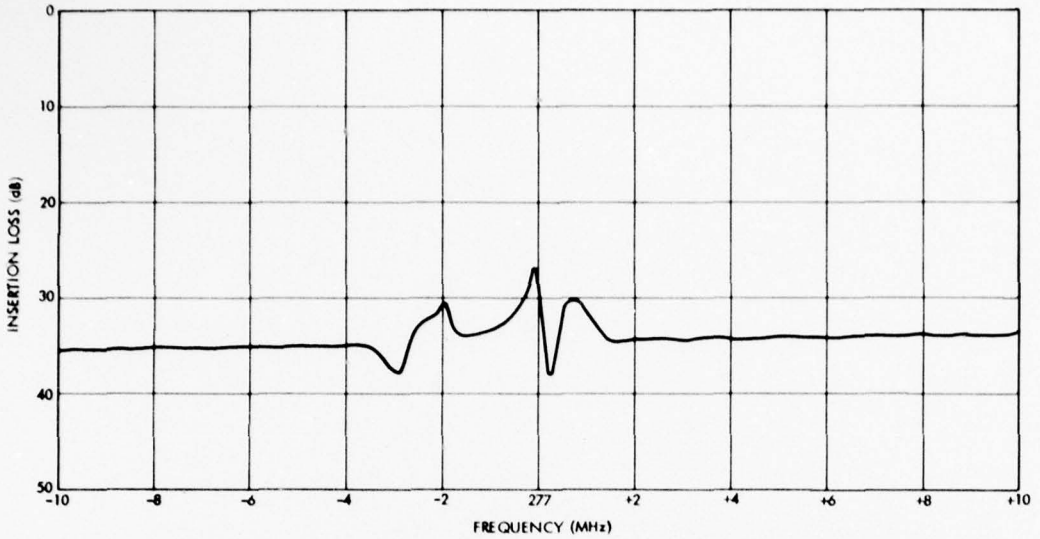

Figure 3-13. 75 Degrees "A" Rotated SAW Delay Line Passband Characteristic

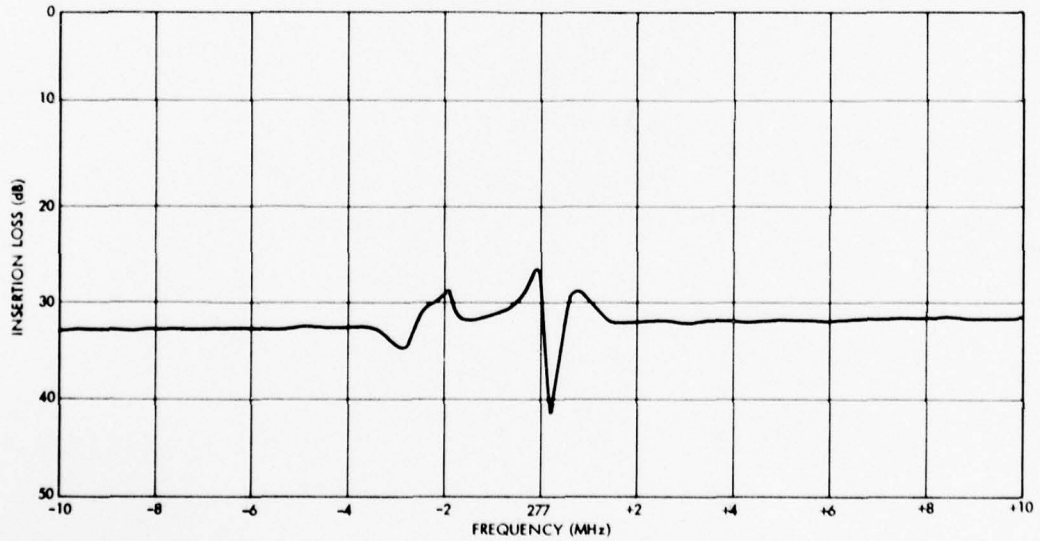

Figure 3-14. 75 Degrees "B" Rotated SAW Delay Line Passband Characteristic

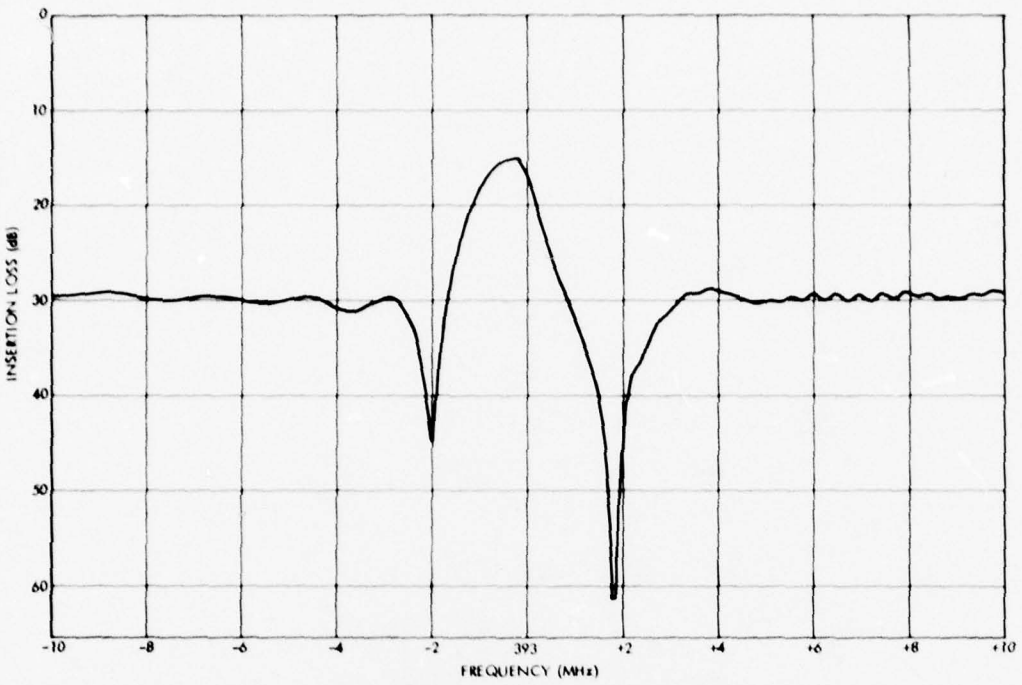

Figure 3-15. 90 Degrees "A" Rotated SAW Delay Line Passband Characteristic

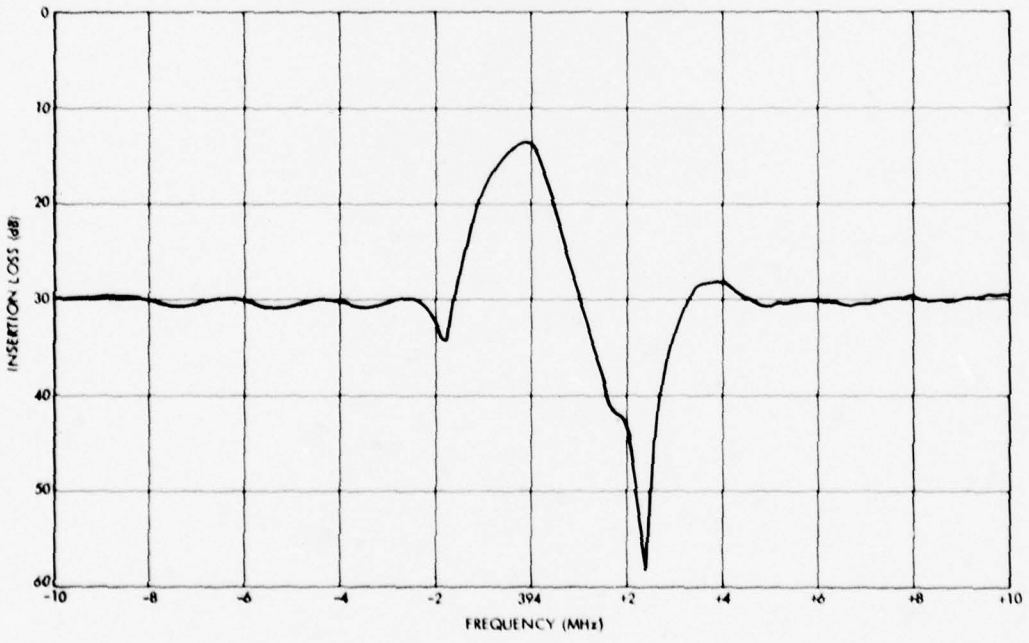

Figure 3-16. 90 Degrees "B" Rotated SAW Delay Line Passband Characteristic

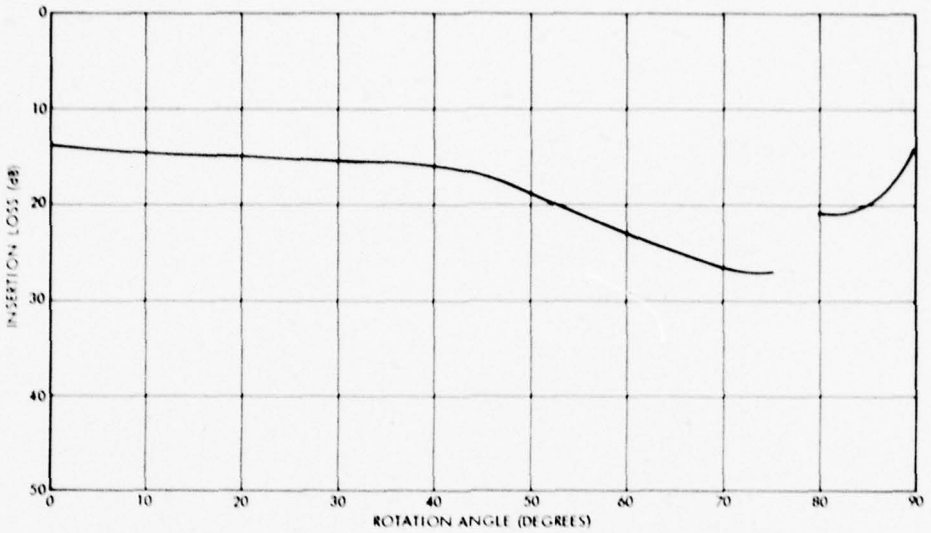

Figure 3-17. SAW Delay Line Insertion Loss as a Function Rotation

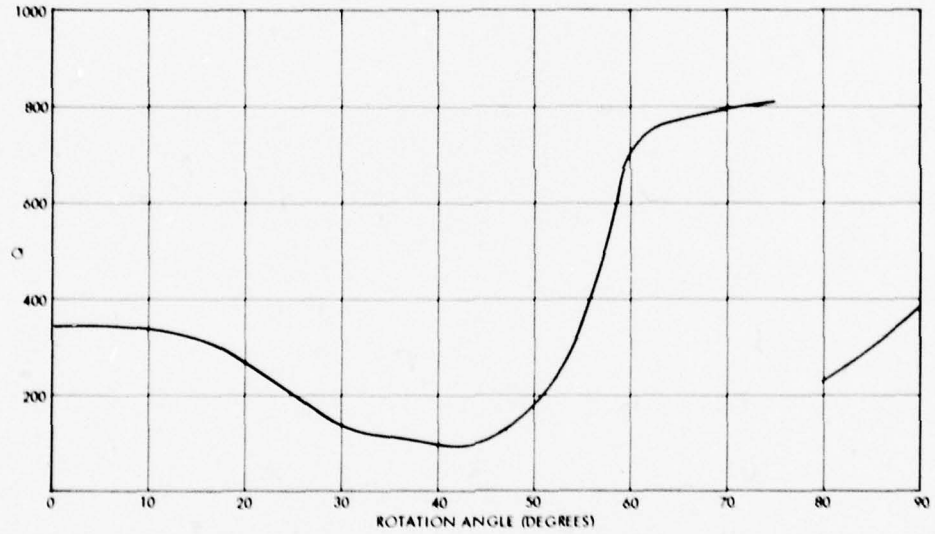

Figure 3-18. SAW Delay Line Q as a Function of Rotation Angle

For rotation angles of greater than 45^{o}, the passband became severely distorted and the insertion loss increased by approximately 10 dB over the 0^{o} rotation value of 14 dB. There was also significant skewing of the response which resulted in multiple responses in the passband. These multiple responses tended to reduce the bandwidth of the main SAW response and hence the increase in Q from a nominal value of 357 for the 0^{o} rotation to 714 for the 75^{o} rotation. It should be noted, though, that the passband distortion did not interfere with the use of the rotated SAW delay lines in a SAW oscillator configuration.

3.2.3 Temperature Coefficient

The temperature stability of the SAW delay lines has also been found to be a function of rotation angle. This dependence is graphed in Figure 3-19. As can be seen from the graph, the relationship between first order temperature coefficient and rotation angle is a complex function. For the nominal 0^{o} rotation, the first order coefficient was zero, as is to be expected. Between 0^{o} and 48^{o}, the first order coefficient is positive with a maximum value of 12.6 ppm/^{o}C for a rotation of 30^{o}.

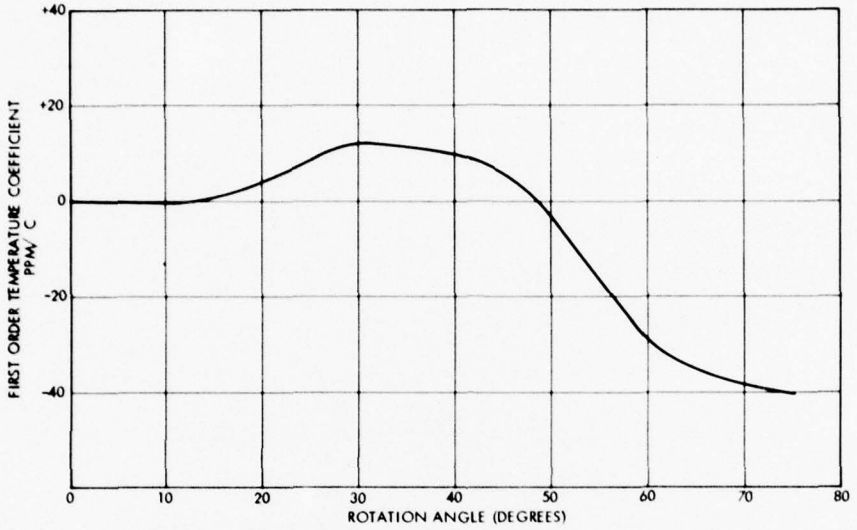

Figure 3-19. SAW Delay Line First Order Temperature Coefficient as a Function of Rotation

Extrapolating the measured data indicates that the first order coefficient will go to zero for an angle of approximately 48^{o}. For rotation angles of 48^{o} to 75^{o}, the coefficient is negative, with a maximum value of -40 ppm/^{o}C at 75^{o}.

The single data point for the 90^{o} rotated delay lines is not plotted on the graph because, as previously described, these delay lines did not operate in a surface acoustic wave mode. The basic dependence of frequency vs temperature for the 90^{o} rotation was linear with a coefficient of +30 ppm/^{o}C. The frequency vs temperature plots for the 14 SAW delay lines are shown in Figures 3-20 through 3-33.

ST-cut quartz has a parabolic frequency vs temperature characteristic with a null at about room temperature. A useful side benefit of rotating the delay line is the ability to increase the temperature at which the zero occurs. For example, the zero for the 15^{o} rotation occurred at approximately 95^{o}F, a 45^{o}F increase over the 0^{o} rotation. This effect could be particularly useful for higher frequency SAW delay lines. Due to second order effects, the zero temperature for typical 1 GHz SAW delay lines is reduced to about 30^{o}F. By rotating the delay line, this effect could be compensated.

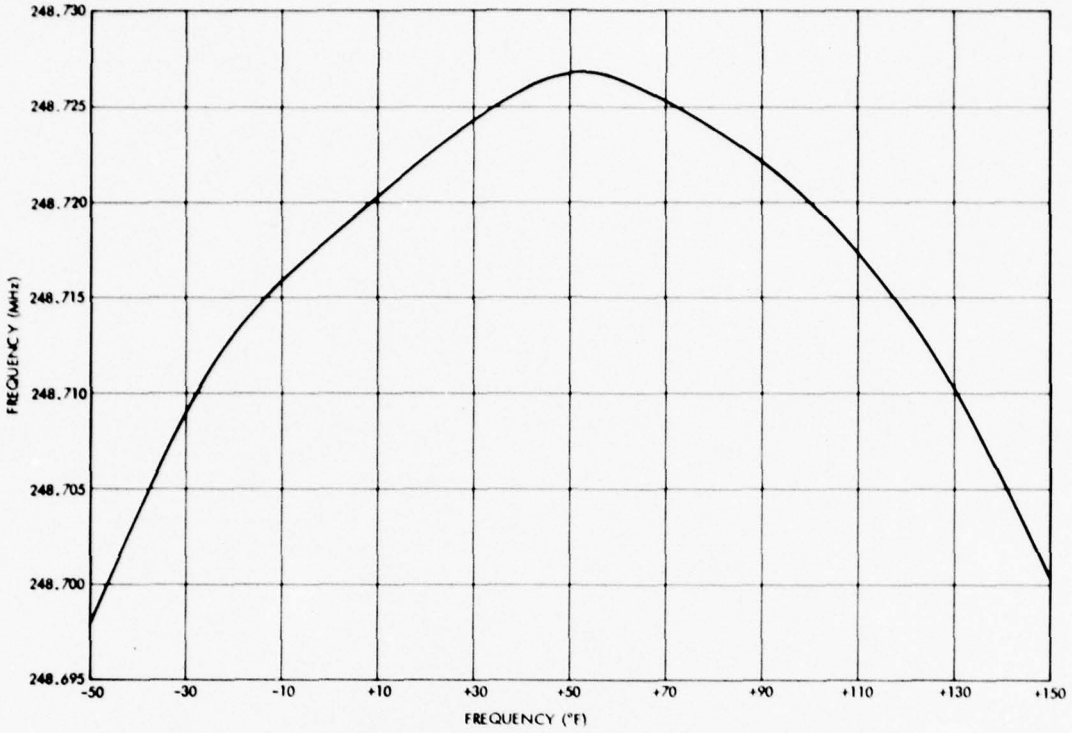

Figure 3-20. 0 Degree "A" Rotated SAW Delay Line Measured Temperature Stability

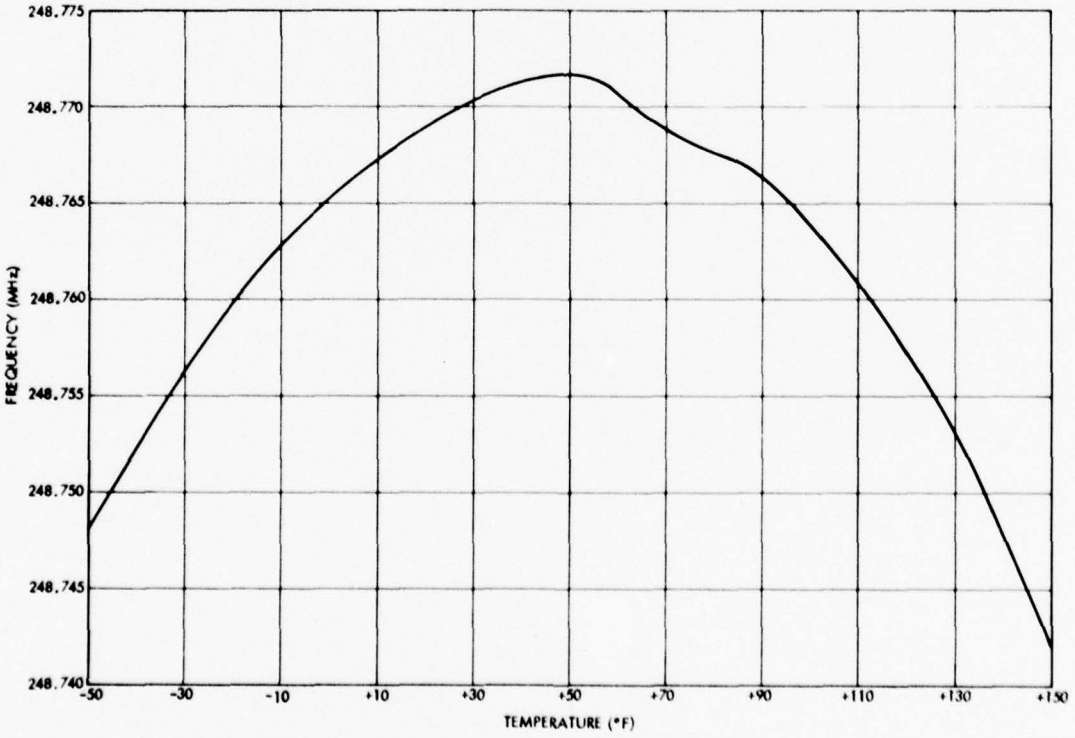

Figure 3-21. 0 Degree "B" Rotated SAW Delay Line Measured Temperature Stability

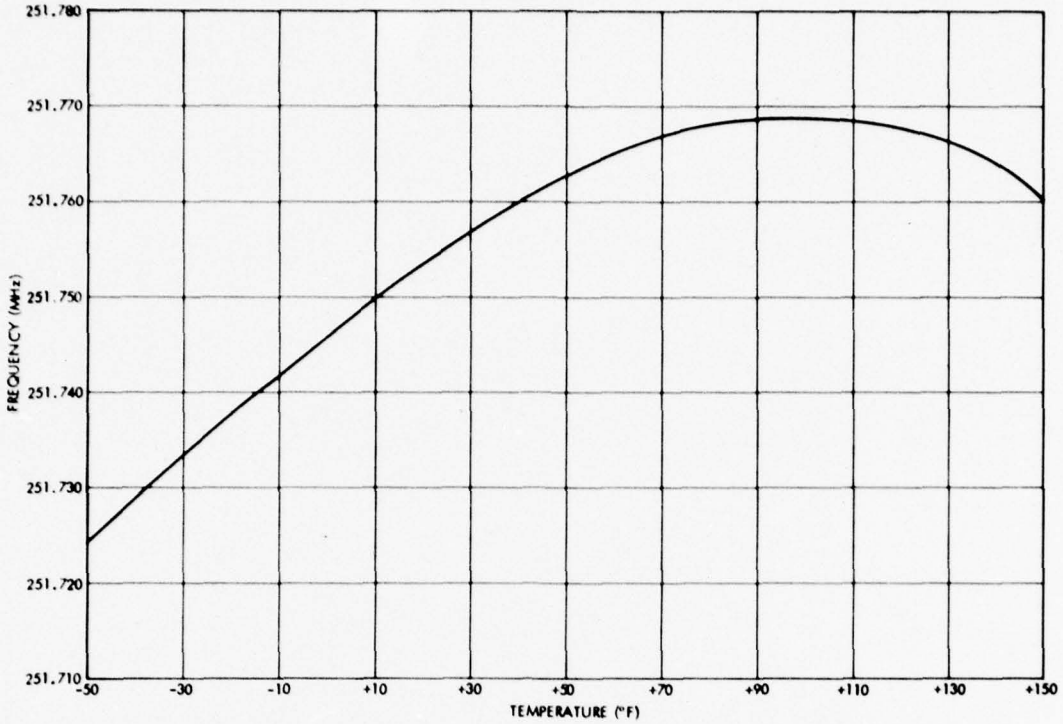

Figure 3-22. 15 Degrees "A" Rotated SAW Delay Line Measured Temperature Stability

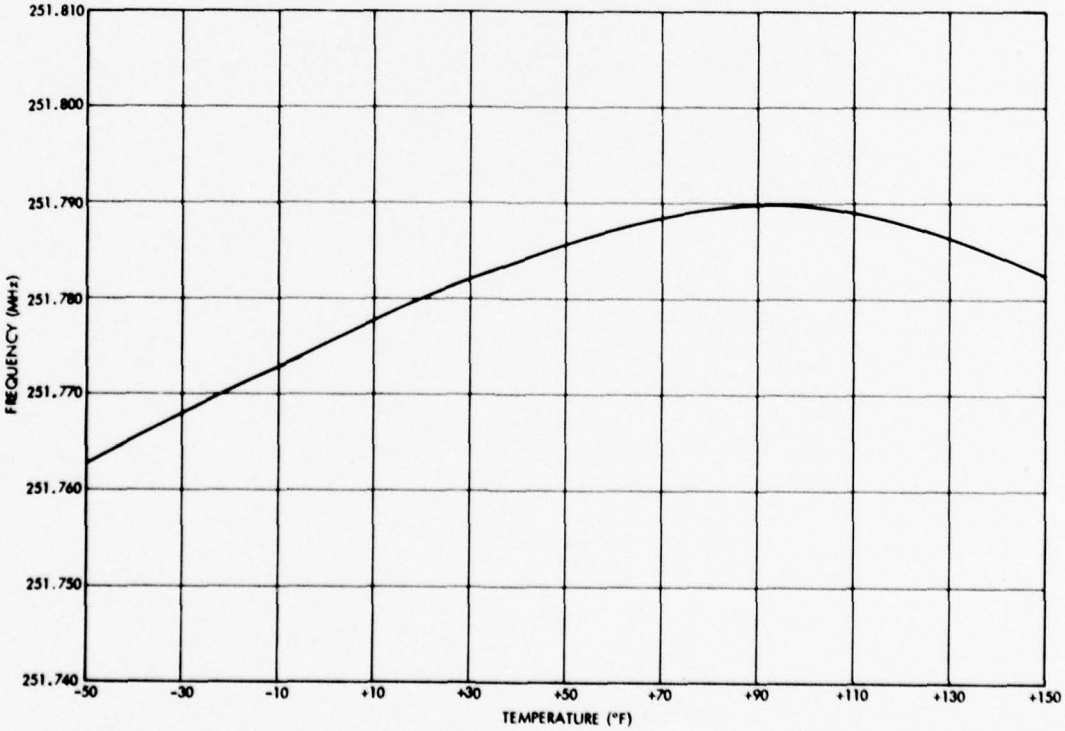

Figure 3-23. 15 Degrees "B" Rotated SAW Delay Line Measured Temperature Stability

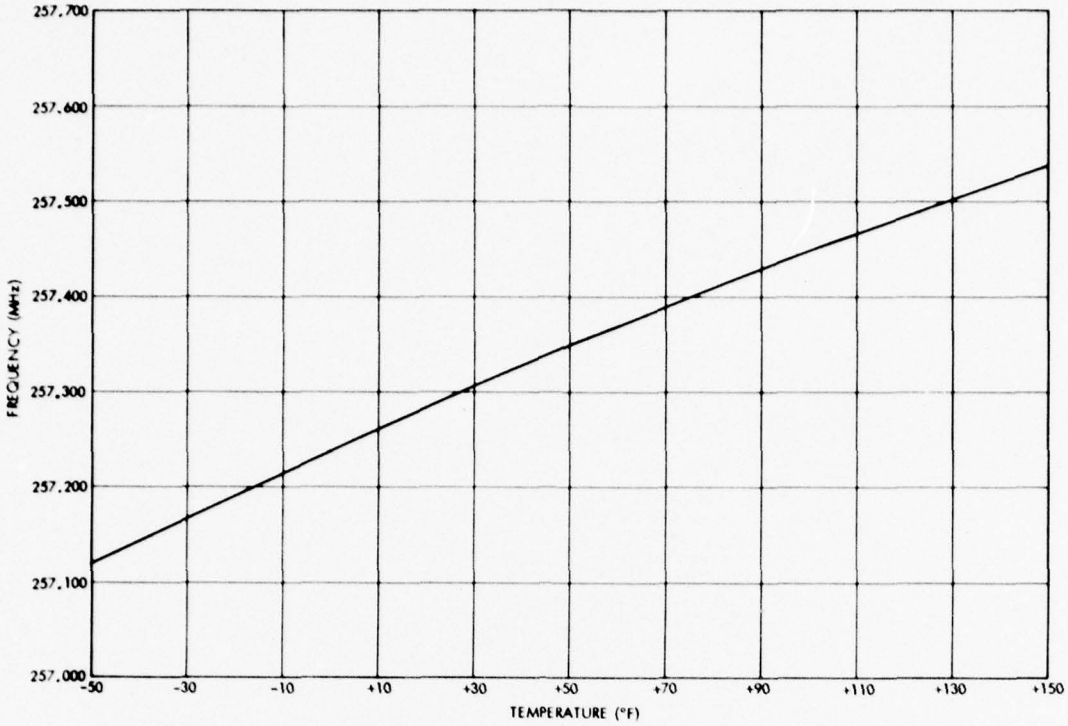

Figure 3-24. 30 Degrees "A" Rotated SAW Delay Line Measured Temperature Stability

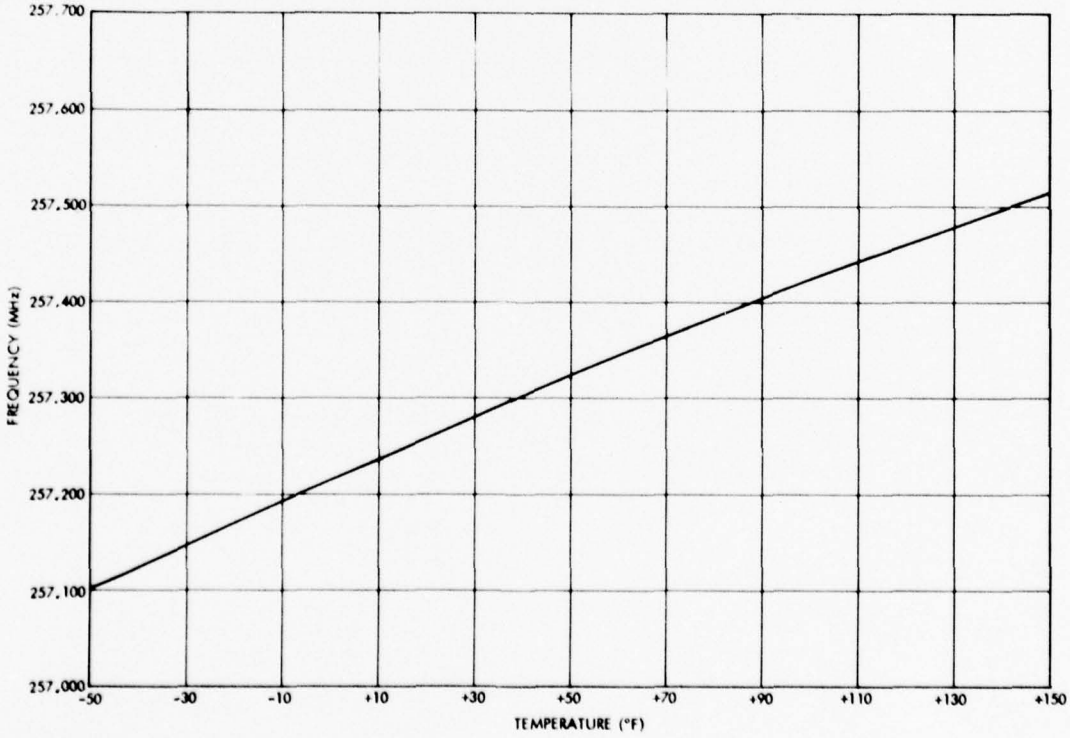

Figure 3-25. 30 Degrees "B" Rotated SAW Delay Line Measured Temperature Stability

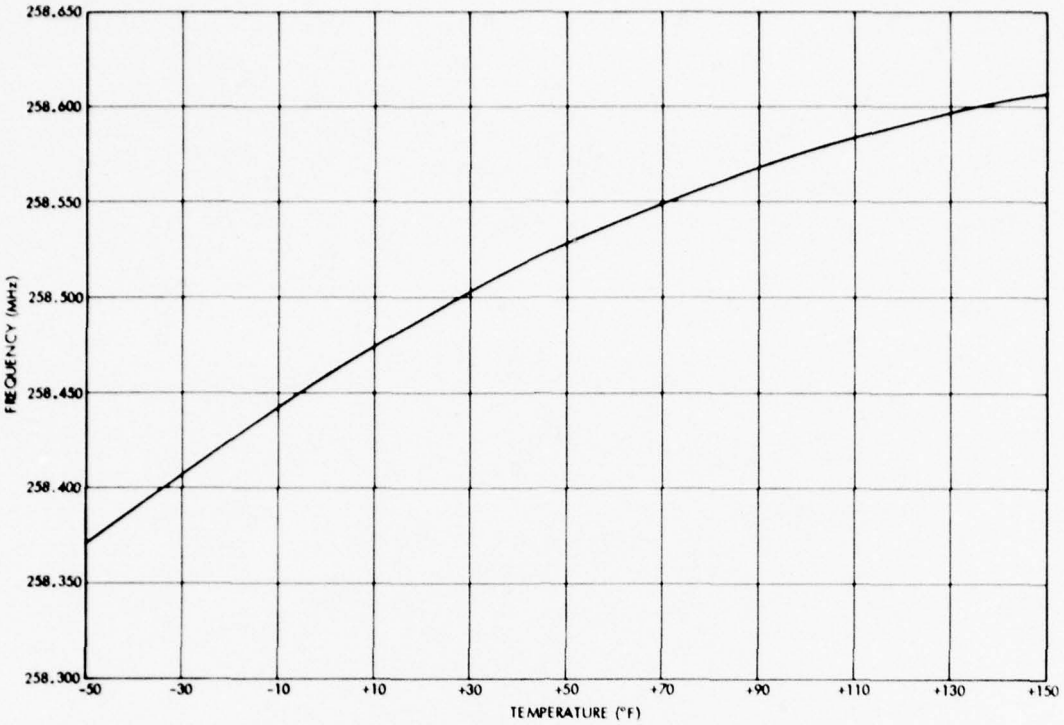

Figure 3-26. 45 Degrees "A" Rotated SAW Delay Line Measured Temperature Stability

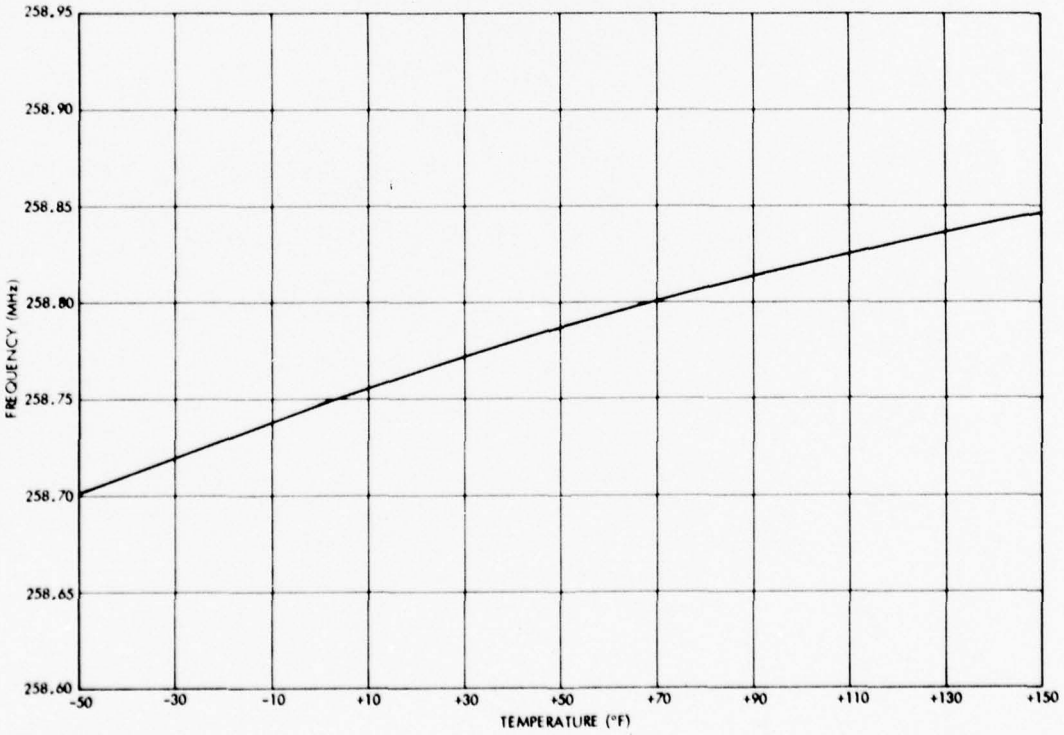

Figure 3-27. 45 Degrees "B" Rotated SAW Delay Line Measured Temperature Stability

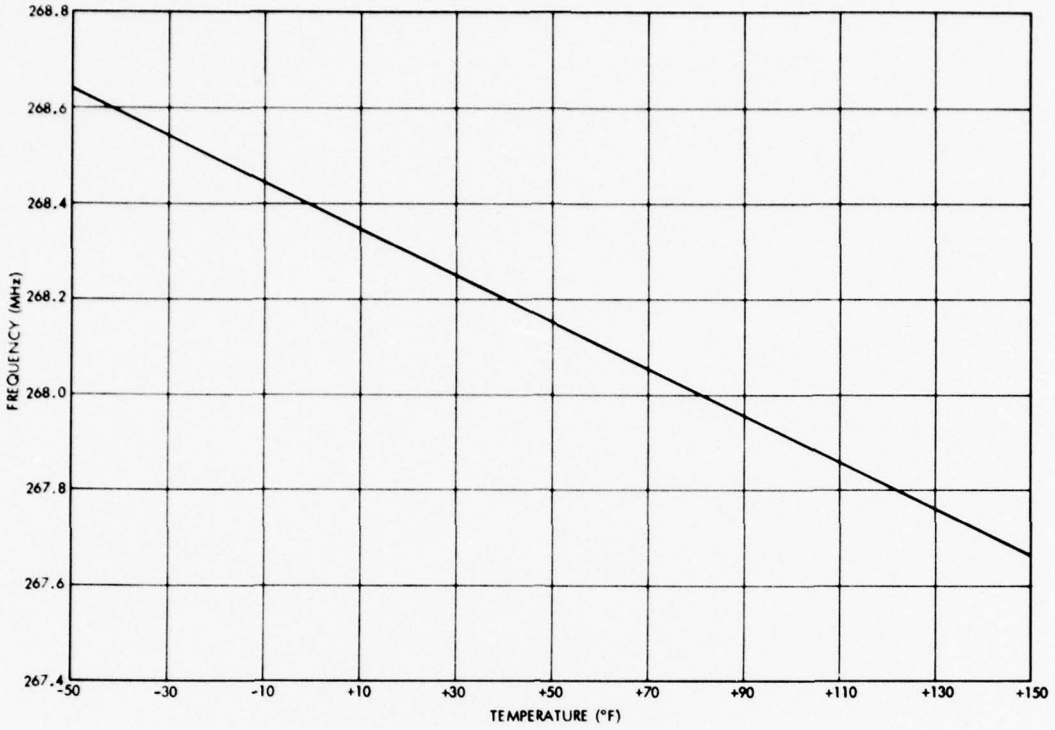

Figure 3-28. 60 Degrees "A" Rotated SAW Delay Line Measured Temperature Stability

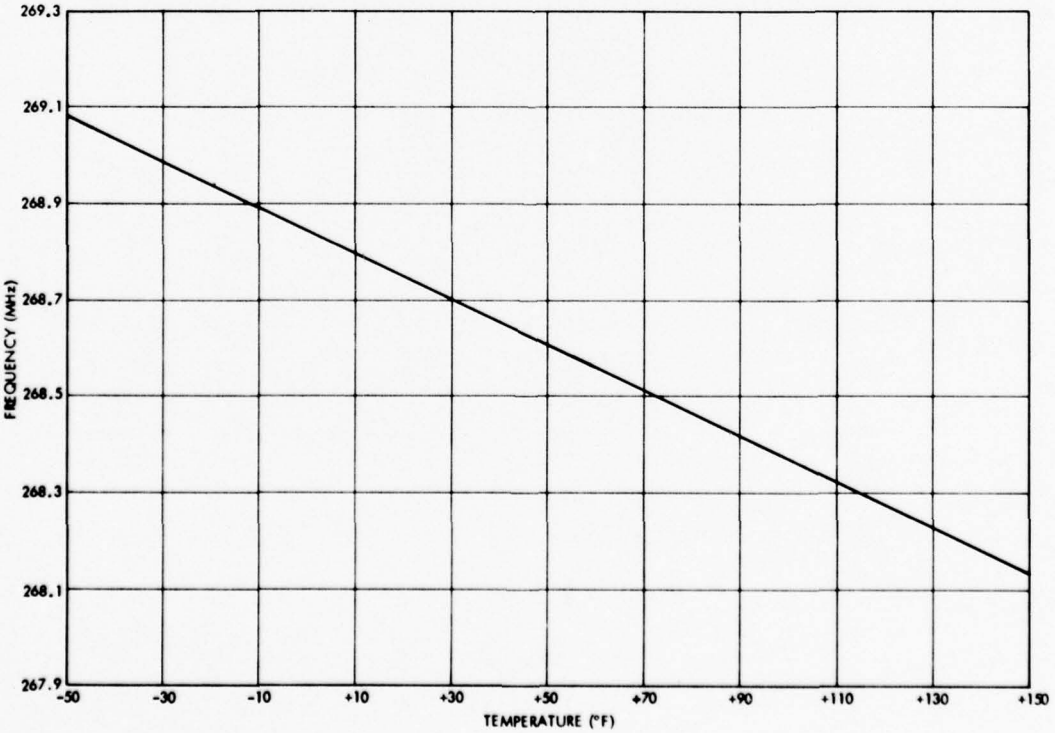

Figure 3-29. 60 Degrees "B" Rotated SAW Delay Line Measured Temperature Stability

Figure 3-30. 75 Degrees "A" Rotated SAW Delay Line Measured Temperature Stability

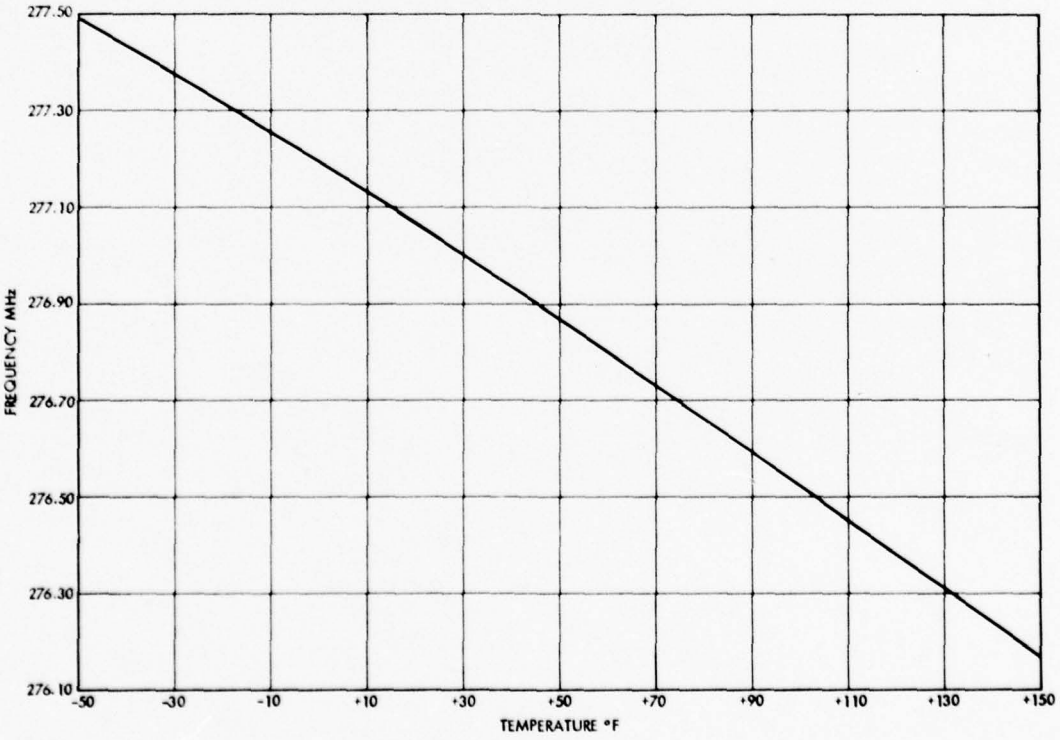

Figure 3-31. 75 Degrees "B" Rotated SAW Delay Line Measured Temperature Stability

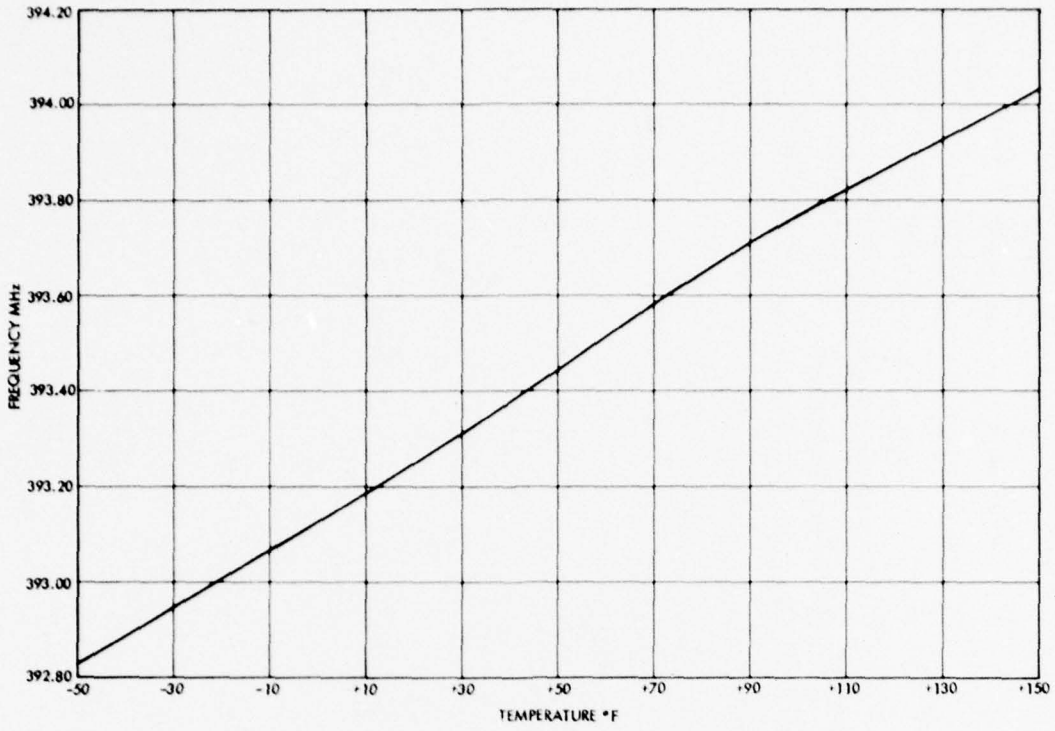

Figure 3-32. 90 Degrees "A" Rotated SAW Delay Line Measured Temperature Stability

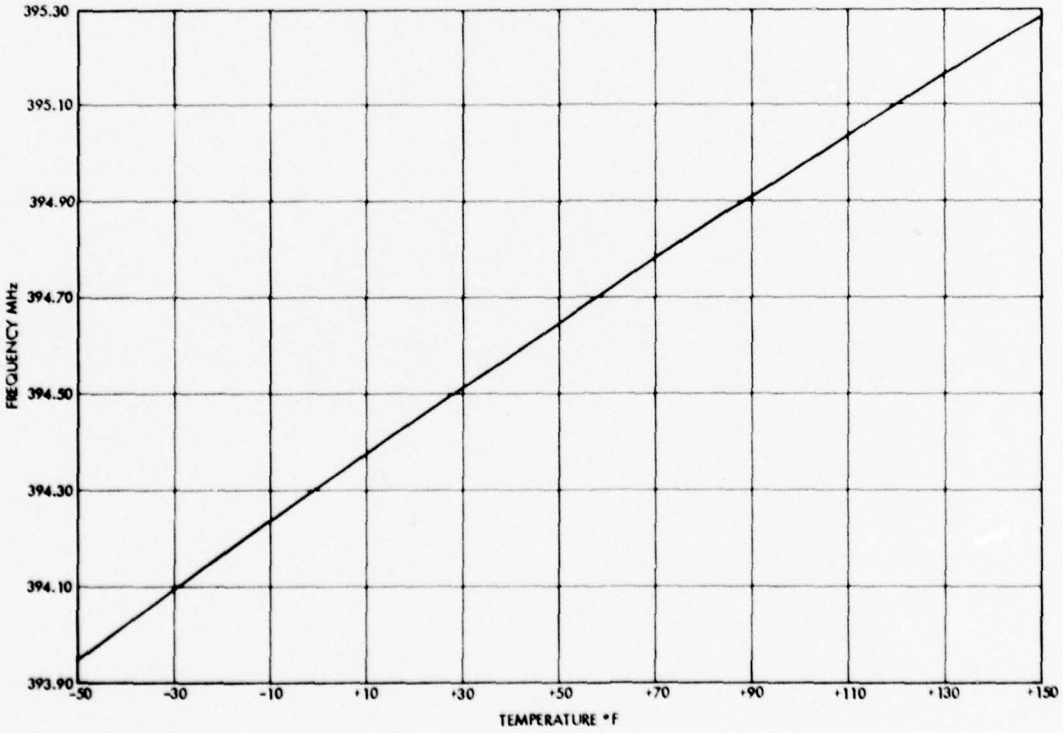

Figure 3-33. 90 Degrees "B" Rotated SAW Delay Line Measured Temperature Stability

4. SAW OSCILLATOR DESIGN AND FABRICATION

This section discusses the theory of SAW oscillator operation and describes the way in which this theory was implemented for the program.

4.1 THEORY OF OPERATION OF SAW OSCILLATORS

A SAW oscillator consists of a SAW delay line connected in a feedback loop with an amplifier as shown schematically in Figure 4-1. This circuit oscillates at any frequency for which the total phase shift around the loop is an integer multiple of 2π, and the gain of the amplifier is equal to or greater than the net insertion loss of the feedback elements. The conditions for oscillation can be expressed as

$$\frac{2\pi f \ell}{V} + \phi = 2n\pi \tag{4.1}$$

and

$$L_S(f) + L_1(f) = G(f, A) \tag{4.2}$$

where

f = oscillation frequency
ℓ = center to center transducer separation
V = surface wave velocity
ϕ = phase shift through all elements except SAW delay line
n = an integer
$L_S(f)$ = insertion loss of SAW delay line
$G(f,A)$ = amplifier gain as a function of f and output level, A

Solving (4.1) for f

$$f = \frac{V}{\ell}\ n - \frac{\phi}{2\pi} \tag{4.3}$$

As a general rule, $L_1(f)$ and $G(f,A)$ are very slowly varying functions of f over a broad range around the frequency for which the oscillator is being designed, but $L_S(f)$ is a very strong function of frequency. The SAW delay is designed as a bandpass filter whose response is ideally given by

$$L_S(f) = K\left(\frac{\sin X}{X}\right)^2 \left(\frac{\sin Y}{Y}\right)^2 \tag{4.4}$$

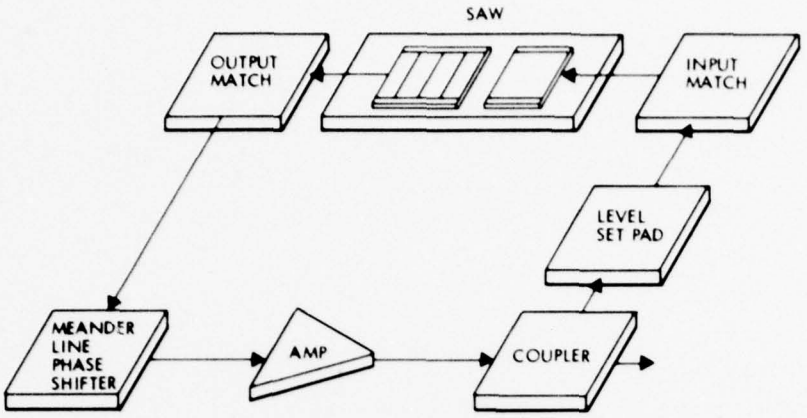

Figure 4-1. Schematic of SAW Oscillator

where

$$X = \frac{2\pi N(f-f_o)}{f_o}$$

$$Y = \frac{2\pi M(f-f_o)}{f_o}$$

K = insertion loss at f_o

N = number of finger pairs in first transducer

M = number of finger pairs in second transducer

$$K\left[\frac{\sin\left(\frac{2\pi N(f-f_o)}{f_o}\right)}{\frac{2\pi N(f-f_o)}{f_o}}\right]^2\left[\frac{\sin\left(\frac{2\pi M(f-f_o)}{f_o}\right)}{\frac{2\pi M(f-f_o)}{f_o}\,1}\right]^2 = G(f_o, A) - L_1(f_o) \qquad (4.5)$$

It is clear that the ideal case will occur when (4.3) is satisfied at f_o. Equation (4.3) has nearly n solutions, but the gain term of (4.5) can be adjusted such that the only simultaneous solutions to both (4.3) and (4.5) occur in the immediate vicinity of f_o. So long as only one solution to (4.3) falls within the primary response of the SAW delay line, single mode operation of the SAW oscillator is guaranteed.

It is also evident from (4.3) that some frequency modulation of the SAW oscillator is possible. Taking the derivative

$$\frac{df}{f} = \frac{-Vd\phi}{2\pi\ell\phi} \qquad (4.6)$$

gives the expected result that the smaller the center-to-center transducer separation, i.e., the lower the delay line Q, the greater the SAW oscillator tuning range. The usual method of accomplishing the tuning is via a phase shift network.

The preceeding has established the design goals for the oscillator circuit, in particular equations (4.3), (4.5), and (4.7). The following discusses the actual implementation of the circuitry surrounding the SAW delay line.

4.2 SAW DELAY LINE FABRICATION

The six SAW delay lines tested in this program were of the open structure configuration as shown in Figure 4-2. This open structure delay line consisted of a normal transducer of 201 fingers and a thinned electrode transducer with five sections, each consisting of 41 fingers. A thinned electrode transducer is similar to the normal type interdigital transducer, except that there are periodic open areas between sets of electrodes to reduce the second order effects. The center-to-center separation between transducers was 500 wavelengths. This path length separation gives the delay line a high Q and enables the SAW oscillator to have good short term stability. This delay line was designed to have a center frequency of operation of about 250 MHz.

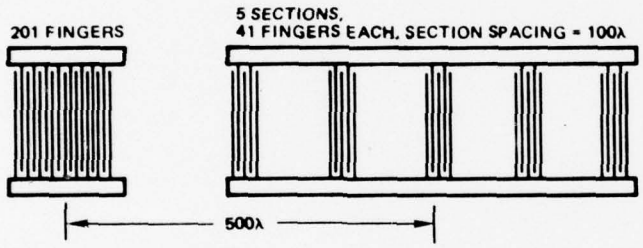

Figure 4-2. Transducer Configuration for SAW Delay Lines

The frequency response of a thin electrode transducer is given as

$$H(f) \propto A \frac{\sin x}{x} \frac{\sin \hat{N}\pi f_o \tau_o}{\sin \pi f_o \tau_o} \quad , \tag{4.7}$$

where

A = a constant related to material constants

$x = N\pi(f-f_o)/f_o$

N = number of finger pairs per section

$\hat{N}$ = number of sections

τ_o = time delay between sections

A delta-function model and an equivalent circuit model were used to simulate delay line characteristics. Calculations were performed on a CDC Cyber 174 computer. The resultant frequency response of the delay line is the product of the two individual transducer transfer functions. The calculated frequency response is shown in Figure 4-3.

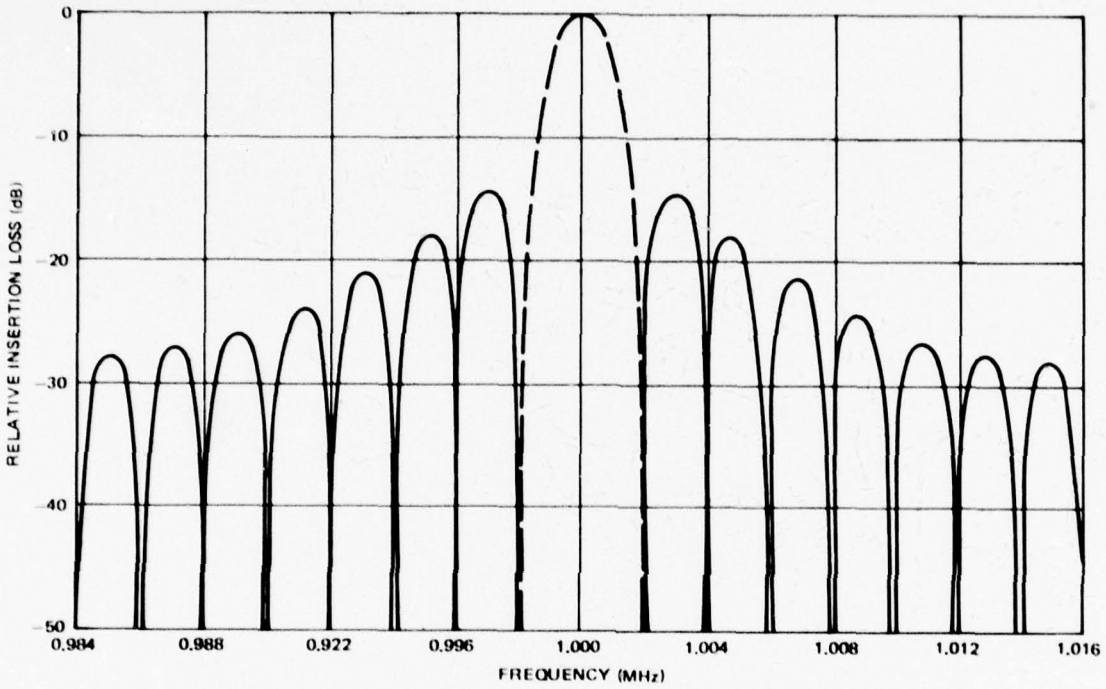

Figure 4-3. Theoretical Frequency Response of the SAW Delay Line

The original mask for the 250 MHz SAW delay line was fabricated on a standard 60-mil thick glass plate coated with anti-reflecting chrome. This photomask was then transferred to a conformal flexible photomask of 7-mil thickness. A vacuum frame with a thin rubber membrane was used to lift the quartz substrate into intimate contact with the flexible mask. This minimized diffraction effects which occurred during the ultraviolet exposure of the photoresist, thus ensuring good linewidth resolution for the transducers.

The photolithographic technique used in the fabrication of the interdigital transducers is illustrated in Figure 4-4. The transducer patterns were fabricated by the "etching" technique. In etching, a thin metal film is deposited on the substrate followed by spin or dip coating of Shipley 1350J positive photoresist. The surface is then exposed with a highly uniform monochormatic UV light source through a light field photomask. After exposure, the surface is developed, forming a transducer pattern over the metal film. The metallic pattern is defined by chemically etching or sputter etching through the developed photoresist pattern.

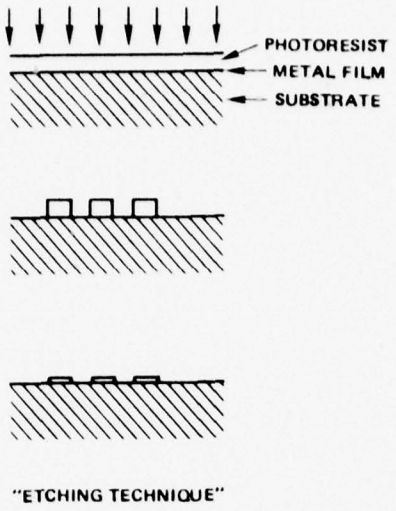

Figure 4-4. Schematic Illustration of the Planar Fabrication Techniques

Prior to the metallization, all the quartz substrates were baked at 200°C for 30 minutes, and then slowly cooled to room temperature under vacuum. This was done to minimize the amount of absorbed gases which might otherwise be trapped on the quartz substrate surface by the metal film. The metal films for the chrome/aluminum transducers were formed by flash evaporating about 75 Å of chromium followed by the evaporation of about 1250 Å of aluminum. The chrome/gold metallization consisted of about 50 Å of chromium and 500 Å of gold. A thin layer of gold (500 Å) was used to minimize the mass loading effects associated with thick gold films. These films were evaporated at low substrate temperature in order to minimize the grain size. The chromium films were used to ensure good adhesion of the aluminum and gold films.

Chemical etching and ion milling techniques were evaluated for fabrication of the Cr/Au transducer patterns. Two chemical etchants were investigated. The standard semiconductor gold etchant, (400 g KI, 100 g I_2, and 400 ml of water) was tried first. After dilution with water, this etchant had a high etching rate (≈500 Å/sec) and it destroyed the photoresist pattern. The second etchant, which was successful in producing delay lines, was a commercial chemical called Technistrip. After diluting Technistrip with water, a controllable etching rate of approximately 50 Å/sec was obtained. The samples were etched for 10 seconds in diluted Technistrip heated to 50°C. This etching procedure yielded the best SAW delay lines.

A Veeco Microtech system was also used to etch the samples. The delay lines produced by ion milling had excellent line edge resolution. The approximate etching rate was 27 Å/sec at the standard operating conditions of the system. The ion-milled delay lines were not used for the aging studies since this technique is not readily amenable to mass production methods.

4.3 TEMPERATURE CYCLED OSCILLATOR FABRICATION REVIEW

The four 250 MHz SAW oscillators which were temperature cycled were fabricated as part of a related contract (N00123-75-C-1182). The following reviews their fabrication.

All of the SAW oscillators were assembled using the same technique. The oscillators consist of a hermetically sealed matched SAW delay line, an amplifier substrate, and a meander line phase shifter substrate. All of the components are mounted in a single machined aluminum chassis. Figure 4-5 is a photograph of a completed 250 MHz oscillator. The lid and clamp for the delay line package have been removed for clarity.

The amplifier and meander line phase shifter were both fabricated on alumina microstrip circuits. The amplifier is contained in a hermetic 22-pin package. The package is mounted on the ground plane side of the substrate using conductive epoxy. The power divider, attenuator, bias bypass capacitors, and interconnecting circuitry are all on the top side of the substrate. The meander line substrate is simply a number of 50 ohm lines of various lengths. The different lines are then interconnected using ribbons to select the required phase shift. Both substrates are mounted on Kovar carriers which are attached to the oscillator chassis with screws. Spring finger frames under each substrate ensure a good ground contact between the substrate ground plane and the chassis.

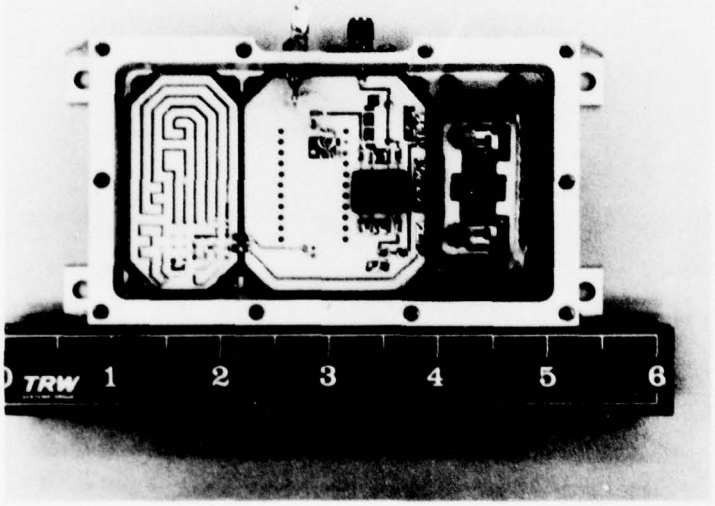

123095-5

Figure 4-5. 250 MHz SAW Oscillator

An Aertech type AMT 5010 multistage thin film MIC amplifier was used as the gain element in the four test oscillators. The broad bandwidth (200 to 600 MHz), high gain (>30 dB), and low noise figure (<1.9 dB at 250 MHz) of the amplifier were specified to ensure optimum oscillator performance. Each stage of the amplifier was carefully optimized with respect to gain, noise figure, and output power for use in the SAW oscillator. The amplifier was packaged in a single 1 x 0.5 inch dual-in-line hermetic package.

The thin film design was chosen because of its excellent electrical performance, high temperature stability, and small size.

The remaining components required for the oscillator are all straightforward. A commercial 3 dB power divider (ANZAC DS-109) was used to couple a portion of the amplifier output back through the SAW delay line. The device is broadband (10 to 500 MHz). The attenuator in the feedback loop is simply a "TEE" configuration attenuator utilizing thin film chip resistors. The values of the resistors were selected to provide the required level of attenuation.

The total loop phase shift (or oscillator frequency) is fine tuned by a meander line phase shifter. The total length of the line is varied by interconnecting lines of different lengths. Relative phase shifts of up to 360^{o} in 2.5^{o} increments can be selected at 250 MHz. A variable capacitor network could have been used to perform this function, but the temperature stability of the oscillator would have been degraded.

A common requirement for all of the electronics in the oscillator loop is the stability of the insertion phase and gain or loss of each component. All of the components used in the oscillator were selected for maximum temperature and long term stability. In order for the aging tests to accurately reflect the aging in the SAW delay lines, the long term stability of the remaining components in the oscillator must be significantly better than the SAW crystal.

The four SAW delay lines were matched to 50 ohms at the input and output. Both the delay line and matching network were mounted in a hermetic flatpack on an alumina carrier. Figure 4-6 is a photograph of an assembled 250 MHz delay line prior to sealing. The delay lines were hermetically sealed to protect the surface of the crystals. The center frequency of the delay lines is very sensitive to any contamination (particularly moisture) on the surface of the delay line. In addition to protecting the face of the SAW crystal, the packaging technique for the delay line must also protect the crystal from mechanical stresses. The quartz crystal was attached to the alumina carrier with Dow Corning RTV No. 6-1104. This material is particularly suited to this application for the following reasons. First, the material exhibits a minimum of outgassing. This is important to prevent contamination of the SAW crystal after it is sealed. Second, the material is flexible and acts as both a mechanical shock absorber for the crystal and absorbs the stresses due to the different thermal coefficients of expansion of the quartz crystal and the alumina carrier. Finally, the material is used to absorb the acoustic waves which reach the edges of the SAW crystal and would otherwise be reflected back to the transducers.

Electrical connections to the transducers were made using ultrasonically bonded aluminum wires. Thermal compression boding was not used due to the requirement that the SAW crystal be preheated to a high temperature prior to bonding. The chip capacitors and inductors were attached to the carrier using a silver filled conductive epoxy.

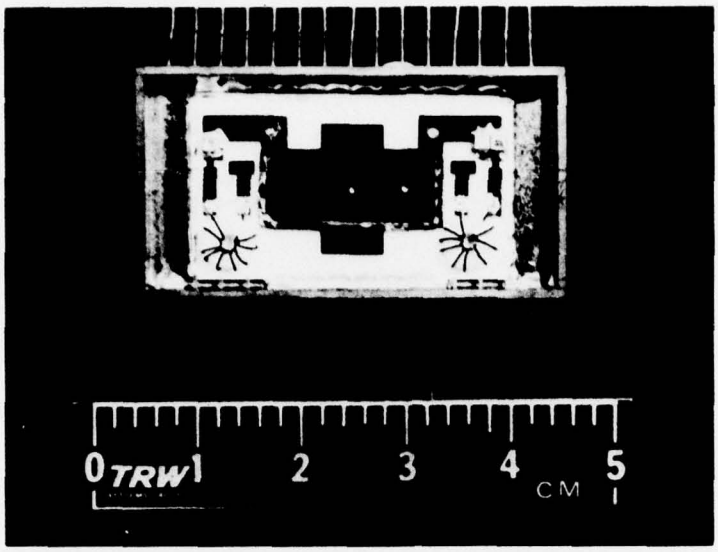

Figure 4-6. 250 MHz SAW Delay Line Prior to Hermetic Sealing

This material was also selected for minimum outgassing. The components were not soldered due to the possiblity of flux or solder contaminating the delay line. Finally the entire carrier was mounted in the flat pack using the same conductive epoxy that was used to attach the chip components. The input and output connections were made by wire bonding from the carrier pads to the leads of the package.

The processing steps followed to seal the delay lines were carefully chosen to ensure that the delay lines are kept as clean and as dry as possible. The crystals were first cleaned with a fine camel hair brush and acetone. They were next blown dry with dry nitrogen to clean any dust particles from the packages. The crystals were then vacuum baked for 24 hours at 150°F to further dry the quartz crystal and to minimize the trapped gasses in the RTV and epoxy. Following the vacuum bake, the packages were stored in dry nitrogen until they were hermetically sealed. Finally, the sealed packages were both fine and gross leak checked to confirm that the packaged delay lines were truly hermetically sealed. Following the sealing process, the input and output return loss and the insertion loss of the delay lines were rechecked. In general, no significant degradation was measured due to the sealing process. The insertion loss of a typical delay line is shown in Figure 4-7.

The alignment process for the oscillators is very simple. The first step is to determine the difference between the delay line insertion loss and the linear amplifier gain. The attenuator in the loop is then selected to provide approximately 3 dB of excess gain in the loop. The amount of excess linear amplifier gain determines the level of saturation in the amplifier when the loop is oscillating. Regardless of the amount of excess linear loop gain, when the loop is oscillating, the amplifier will saturate or compress until the total gain around the loop is reduced to unity.

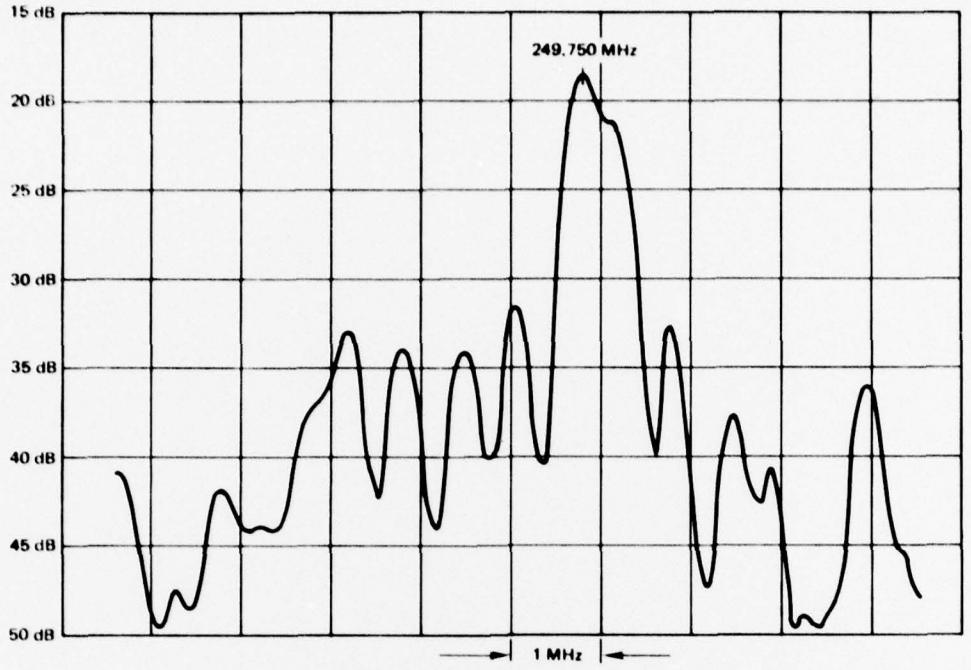

Figure 4-7. SAW Delay Line Insertion Loss SN 107

The 3 dB value of excess loop gain is a compromise between several factors. A higher level of excess gain in the loop would result in greater output power from the oscillator and would provide a greater assurance that the loop will continue to oscillate as the delay line insertion loss increases or the amplifier gain decreases due to the effects of aging and temperature. However, high levels of excess loop gain and therefore saturation result in an increase in the amplifier noise figure (or oscillator phase noise) and in higher levels of harmonically related spurious outputs.

The second step in aligning the oscillators is to adjust the total loop phase shift. The oscillator is first tested with a nominal amount of extra phase shift. The output frequency is then fine tuned either up or down to the exact desired frequency by either decreasing or increasing the total length of the meander line. Using this technique, the oscillators can be adjusted over a range of approximately ±100 kHz with a resolution of approximately ±5 kHz. Table 4-1 summarizes the data for the 250 oscillators following their initial alignment. In each case, the output frequencies of the oscillators were adjusted to correspond to the frequency of minimum insertion loss of the SAW delay used in the oscillator; i.e., to the f_0 referred to in equations (4.4) and (4.5).

Table 4-1. SAW Oscillator Performance Summary

Delay Line Serial No.	Amplifier/ Oscillator Serial No.	f_o (MHz)	P_{out} (dBm)	Bias Current at +15 V (mA)
111	SN 23311	249.699	9.9	67
107	SN 23313	249.757	10.2	68
109	SN 23315	249.704	9.2	66
106	SN 23316	249.784	10.0	68

4.4 CHROME/GOLD OSCILLATOR FABRICATION

The two chrome/gold delay line oscillators were fabricated using a commercially available hybrid transistor amplifier module from Watkins-Johnson, part No. A73. The amplifier typically has 32 dB of gain and a 3.5 dB noise figure in the band 5 to 500 MHz, ensuring good performance at 250 MHz. The amplifier performs over the full temperature range of -55°C to +125°C and is packaged in a hermetic TO-5 can. An Anzac DS-109 3 dB power divider was used to couple a portion of the amplifier output back through the SAW delay line. A resistive "TEE" attenuator network was used in the feedback path to set the loop gain. The delay line insertion loss, amplifier gain, and other small losses were used to calculate the value of the attenuator required to realize an excess loop gain of 3 dB. A 10-dB resistive attenuator was included at the output for load isolation, since the loop phase is load dependent. This ensures that the oscillator will see a load VSWR of no more than 1.2:1. A length of 0.031 inch diameter semi-ridgid coaxial line was inserted in the loop to adjust the total loop phase shift and oscillator frequency. A reactive phase shifter was avoided since such a network would have degraded the temperature stability of the oscillator.

The goal in specifying the electronics for the loop was to maximize long-term stability of the loop gain and phase. All of the components used in the oscillator were chosen so that temperature and long term stability of the loop electronics would be significantly better than the stability of the SAW delay line. This ensures that the delay line is the dominant element in determining oscillator frequency and that the frequency measurements reflect primarily the aging of the SAW delay line.

The two oscillators were each assembled in a single machined brass chassis 1.5 by 3.0 inches. The loop electronics were mounted on a small duroid board which was soldered directly to the brass housing. The SAW delay line was mounted in a hermetic 0.8 x 0.8 inch package and attached to the chassis with machine screws. No input or output matching was included in the delay line package. The mounting and wire bonding of the quartz crystal closely duplicates the mounting of chrome/aluminum metallized

delay lines previously life tested. Insertion loss vs frequency of the two Cr/Au delay lines are shown in Figures 4-8 and 4-9. Performance of the oscillators is given in Table 4-2. Typical frequency over temperature performance is shown in Figure 4-10.

Table 4-2. Chrome/Gold Oscillator Performance Summary

Amplifier Serial No.	f_o	P_{out}	Bias Current at +15 V
1A	247.772 MHz	-8.7 dBm	19.3 mA
2E	247.640 MHz	-9.0 dBm	19.3 mA

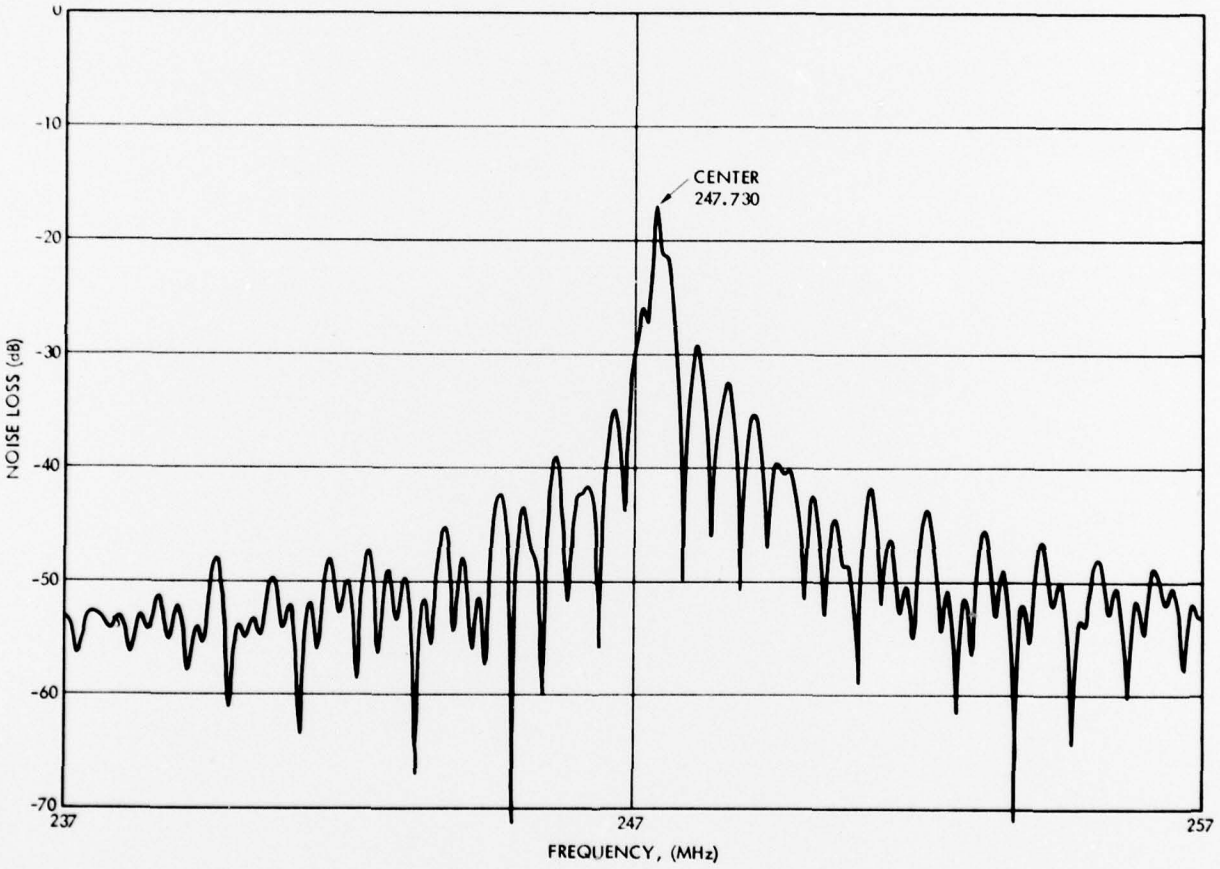

Figure 4-8. Cr/Au SAW Delay Line Insertion Loss SN 1A

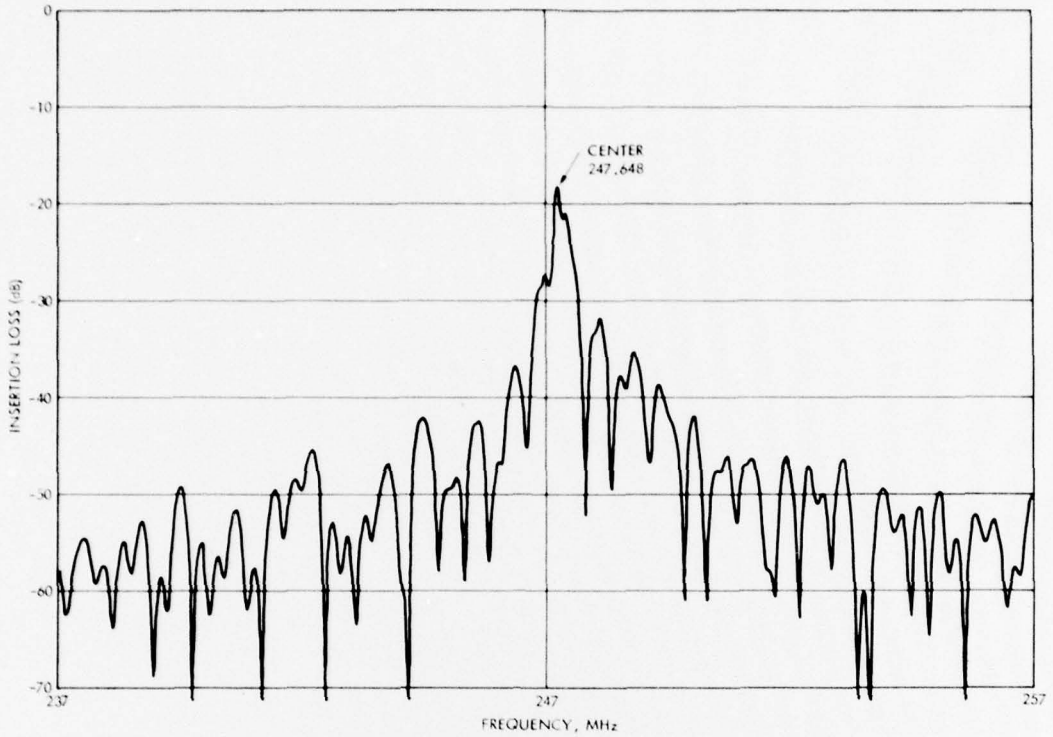

Figure 4-9. Cr/Au SAW Delay Line Insertion Loss SN 2E

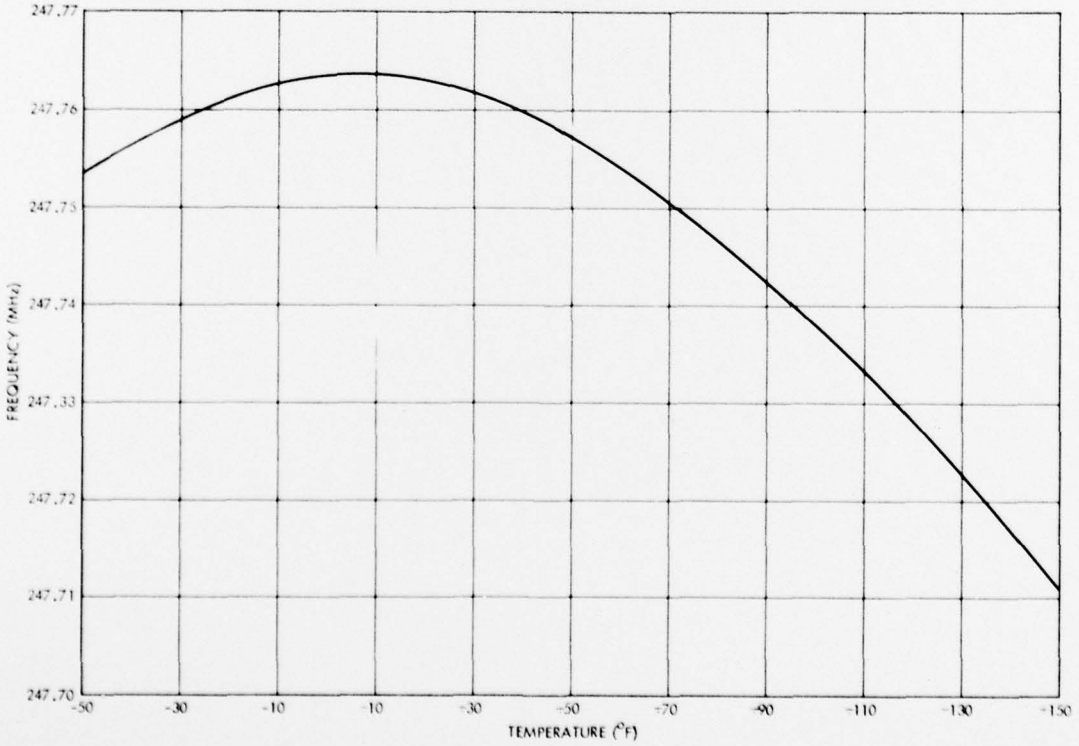

Figure 4-10. Chrome/Gold Metallized Delay Line Oscillator Medium Term Stability SN 1A

5. AGING TEST PROGRAM

TRW has conducted a continuous aging program during the past 2-1/2 years to characterize the aging rate of SAW delay line oscillators. The aging rates of four 250 MHz oscillators have been continuously monitored for the full 2-1/2 year period. In addition, two new oscillators fabricated with chrome/gold metallization have been on life test for 3 months. The aging history of the original four 250 MHz oscillators is shown in Figure 5-1. The four oscillators were first subjected to 12 months of aging tests in a constant environment. A bias cycling test was then performed for 3 months to determine whether the SAW delay line or the oscillator electronics was the major contributor to the overall aging rate. After 6 months of additional stabilized aging, the 3 month temperature cycling test was performed. The oscillators were then again stabilized and further aging data recorded. The total aging rate recorded during each of these tests is summarized in Table 5-1.

5.1 PRE-TEMPERATURE CYCLING AGING REVIEW

The frequency aging rates for the four oscillators during the initial 1 year of continuous life tests are summarized in Table 5-1. The average aging rate for the four oscillators over the 1 year period was -21.0 ppm per year. An additional 18 weeks of data were accumulated. During this 18-week period, the average aging rate for the four oscillators dropped to less than -6 ppm per year. The frequency aging of the oscillators is exponential as evidenced by the decreasing aging rates.

A 3 month bias cycling test was then performed. The purpose was to try to isolate the aging effects in the SAW delay line from those in the remaining loop electronics. Based on existing data for electronic components, the aging rate of the oscillators should be a positive function of temperature; that is, a decrease in temperature should bring about a corresponding decrease in aging rate. The two methods of evaluating the aging characteristics of the SAW oscillators which were considered were to cycle the oscillator bias on and off, or to elevate the oscillator temperature above the baseline value of $92^{o}F$. The first technique was chosen because it offered the potential of separating the aging rate of the delay line from that of the remaining loop electronics. The aging rate of the amplifier alone should decrease when the bias is off whereas the aging rate of the SAW delay line should be independent of amplifier bias. The test was performed by separating the four oscillators into two pairs. One control pair of oscillators was left continuously on. The bias on the other pair was turned off and only turned on once each week – just long enough (≈5 minutes) to measure the oscillator frequency. When the oscillator bias is turned off, the temperature of the delay line drops only a few degrees due to the overall reduction in dc power dissipation and hence oscillator baseplate temperature. The junction temperature of the transistors in the loop amplifier, however, is reduced by $100^{o}F$ due to the thermal resistance of the chip

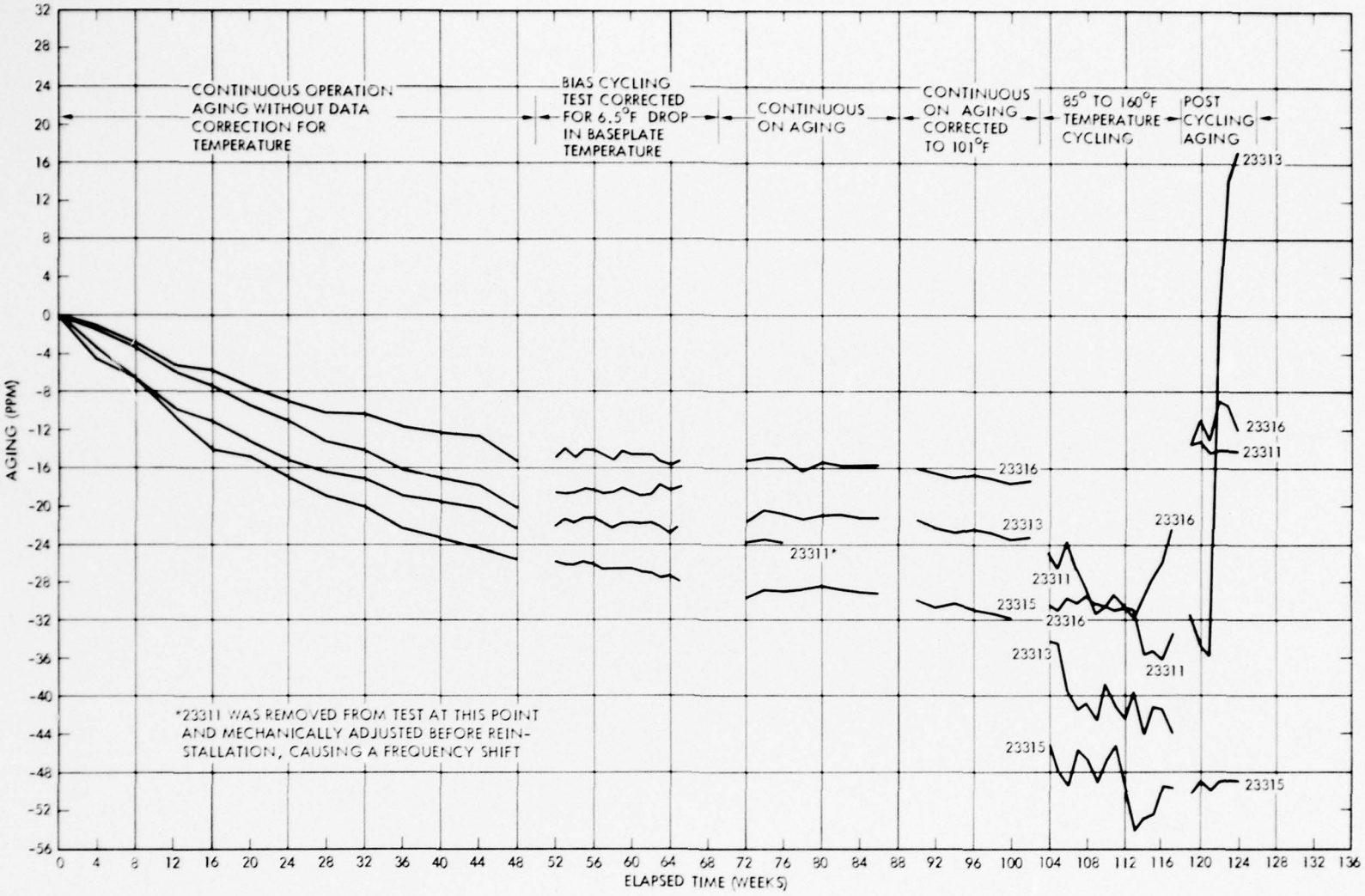

Figure 5-1. SAW Aging Life Tests

Table 5-1. SAW Aging Life Test Summary

Oscillator Serial No.	Continuous Aging			Bias Cycling			Continuous Aging			Continuous Aging With/Temp Correction		
	Aging ppm	Duration Weeks	Aging Rate ppm/yr	Aging ppm/yr	Duration Weeks	Aging Rate ppm/yr	Aging ppm	Duration Weeks	Aging Rate ppm/yr	Aging ppm	Duration Weeks	Aging Rate ppm/yr
23311	-22.2	48	-24.1	- .8	13	-3.2	0	4	0	Not tested		
23313	-20.1	48	-21.8	+ .6	13	+2.4	-.4	14	-1.5	-1.7	12	-7.4
23315	-26.6	48	-28.8	-2.1	13	-8.4	+.2	14	.74	-1.8	12	-7.8
23316	-15.2	48	-16.5	- .9	13	-3.6	-.6	14	-2.2	-1.2	12	-5.2
AVE	21.0	48	22.8	1.1	13	4.4	.4	14	1.5	1.6	12	6.9

Oscillator Serial No.	High-Low Cycling			Continuous Aging			2.5 Year Total		
	Aging ppm	Duration Weeks	Aging Rate ppm/yr	Aging ppm	Duration Weeks	Aging Rate ppm/yr	Aging ppm	Duration Weeks	Aging Rate ppm/yr
23311	-11.2	13	-44.8	+53	5	- 8.3	-16	124	- 7.5
23313	-6.2	13	-24.8	+53	5	551.2	-24	124	-10.1
23315	-4.4	13	-17.6	+ 1	5	10.4	-49	124	-20.5
23316	+3.6	13	14.4	+ 1	5	22.9	-14	124	- 5.9
AVE	6.35	13	25.4	14.2	5	148.82	26.3	124	11.0

transistors. If the two unbiased oscillators had shown a reduction in aging rate compared to the remaining pair of biased oscillators, the results of the test would have suggested that the amplifiers were dominating the oscillator aging; whereas if no significant change in the aging rate had occurred, it would suggest that the delay lines were dominant.

The results of the 13 weeks of bias cycling tests are shown in Figure 5-2. The average aging rate for the continuously biased pair was 5.6 ppm per year, vs 3.4 ppm per year for the on/off biased pair. The slightly different aging rate of the cycled pair is most likely due to thermal transients in the oscillators during turn-on. After bias cycling, the aging rates of the four oscillators returned to the values measured before the test indicating that the bias cycling had an insignificant effect on the oscillator aging. Based on the assumptions made when these tests were started concerning aging mechanisms, it appears that the SAW delay lines are dominating the oscillator aging rate.

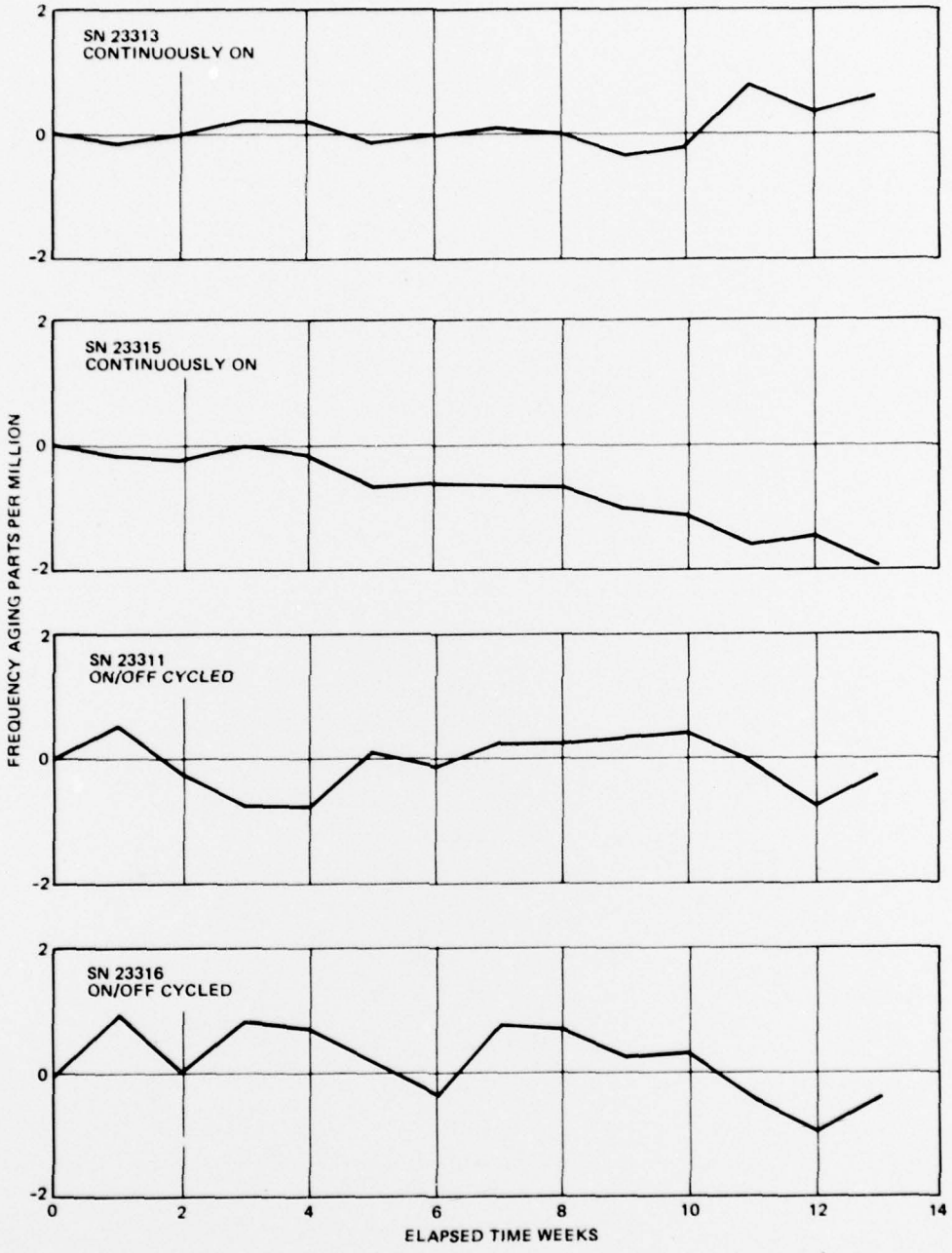

Figure 5-2. SAW Oscillator Bias Cycling Aging Results

During the initial months of the life test, the effect of temperature changes on frequency was small compared to the frequency shift due to aging, and correction of the frequency for the $\pm 1^{o}F$ variations in baseplate temperature was not necessary. As the aging rate decreased, the frequency correction for temperature changes became more significant. In addition, changes in the test configuration caused changes of several degrees in baseplate temperature, such as the $6.5^{o}F$ drop during the bias cycling test, and the $4.5^{o}F$ drop caused by removal of SN 23311 from the test.

A typical frequency vs temperature curve is shown in Figure 5-3. With all four oscillators running, the baseplate temperature was about $101^{o}F$. The best linear correction for temperatures close to $101^{o}F$ is -250 Hz per ^{o}F. Due to the parabolic nature of the frequency dependence on temperature, linear correction is not accurate for temperature differences of more than a few degrees. In order to compare data from different phases of the aging tests, the data shown in Figure 5-1 has been corrected for temperature changes. During the cycling test, the temperature was not allowed to stabilize and the correction for temperature was not very accurate. However, during the post aging test the temperature did stabilize at $101^{o}F$.

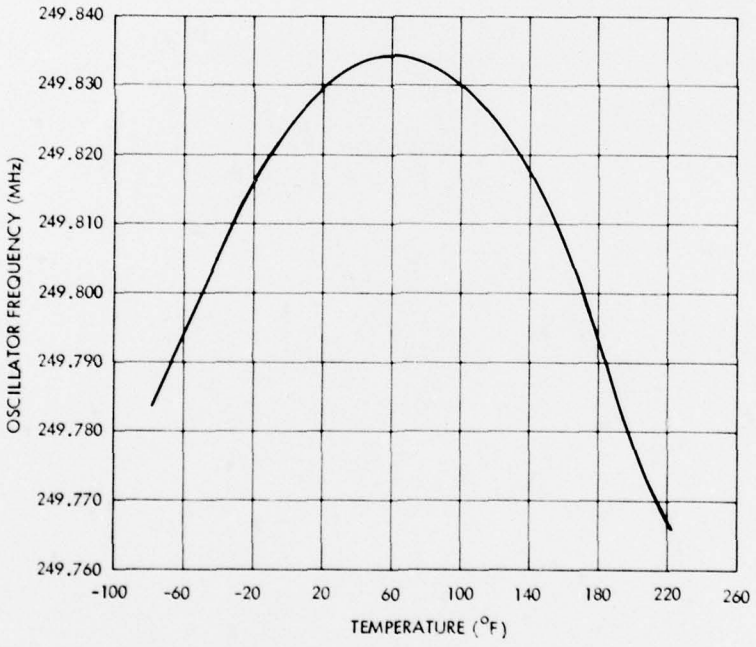

Figure 5-3. Typical 250 MHz SAW Oscillator Medium Term Stability

5.2 TEMPERATURE CYCLING AGING TEST

The four 250 MHz SAW oscillators were subjected to a temperature cycling aging test for a 3 month period. It is well established that the aging rate of electronic components is a function of temperature. The purpose of this test was to determine the magnitude and nature of the relationship between oscillator temperature and aging rate. Performing aging tests at elevated temperatures is a common practice to establish projected long time aging rates. A more stringent form of this type of testing is to temperature cycle the units under test. This not only exposes the circuits to elevated temperatures, but stresses the parts due to the constant heating and cooling. It was therefore felt that the temperature cycling test, which more closely simulates actual operating conditions, would be a more realistic measure of the true aging rate of the SAW oscillators.

The temperature cycling test was configured with the same oscillators and baseplate used in previous tests except that heaters were added to the baseplate. Oscillator SN 23311 was returned to the test, but its frequency changed slightly when several internal mounting screws were retightened.

Thermally conductive rubber heating elements purchased from Electrofilm, Inc., part No. 13000-240, were mounted between the oscillators and the baseplate. The temperature was cycled using a solid state controller which heated the baseplate to 150^{o}F and then allowed it to cool to 85^{o}F. The cycle time was about 2 hours. Frequency was measured on a weekly basis during the low temperature portion of a temperature cycle.

The test continued for 3 months at which time the oscillators were placed in an insulated container and allowed to stabilize, while operating continuously. A comparative record of the cycling test data is shown in Figure 5-4.

During the cycling test, the oscillator frequencies did not track each other. Most of this can be explained by the dynamic character of the test which did not allow the baseplate temperature to stabilize. Temperature gradients in the baseplate could have allowed temperature differences of several degrees between oscillators. This would not have been detected since only one thermometer was used to monitor baseplate temperature. The average aging rate for the four oscillators was about -25 ppm per year during the cycling test, which is about 5 times the -5 ppm per year measured before cycling.

The post cycling aging revealed some unexpected results. After the oscillators were placed in an insulated container and operated continuously, the baseplate temperature was stabilized at 101^{o}F. But the frequency did not return to the values measured before the cycling test. In fact, the cycling test apparently caused unpredictable frequency shifts not related to any external condition such as temperature. This could indicate a different aging mechanism previously not seen. Perhaps the adhesion of the

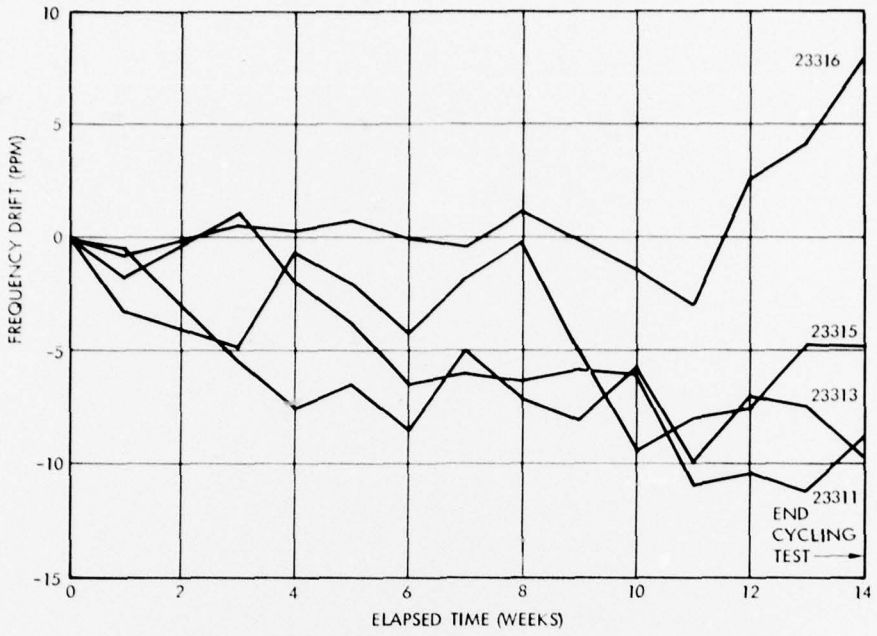

Figure 5-4. Temperature Cycled SAW Oscillator Aging

transducers or stressing at the crystal surface changed during the temperature cycling. To determine more accurately the cause of these shifts in frequency, further carefully planned investigations would be required.

5.3 CHROME/GOLD OSCILLATOR AGING

The aging test of two 250 MHz chrome/gold metallized SAW delay line oscillators began on 8 September 1977. The oscillators were assembled in identical housings using hermetically sealed SAW delay lines. Both oscillators were attached to a common baseplate and placed in a thermally isolated environment. The baseplate temperature stabilized at 91^{o}F with both oscillators operating continuously.

During the aging test, the oscillator baseplate temperature was continuously monitored. The data was taken at the same time each morning. The baseplate temperature varied about ±1.0^{o}F and although the need for temperature correction was minimal, a linear correction of -250 Hz per degree Farenheit was applied.

The frequency aging characteristics of the two oscillators is shown in Figure 5-5. After the first few days, the aging rates of both oscillators were comparable. The aging rate is summarized in Table 3-2 on a monthly basis. The aging of about -60 ppm per year during the fourth month is twice what was measured after 4 months of burn-in for the aging study using chrome/aluminum metallized delay lines. The projected aging rate based on this test would be about -60 ppm per year, compared to the -5 ppm per year measured on chrome/aluminum metallized delay lines.

Table 5-2. Chrome/Gold Oscillator Aging Summary

Oscillator	1st Month	2nd Month	3rd Month	4th Month
2E	-31.8 ppm	-6.5 ppm	-4.5 ppm	-5.5 ppm
1A	-23.5 ppm	-8.0 ppm	-4.5 ppm	-5.5 ppm

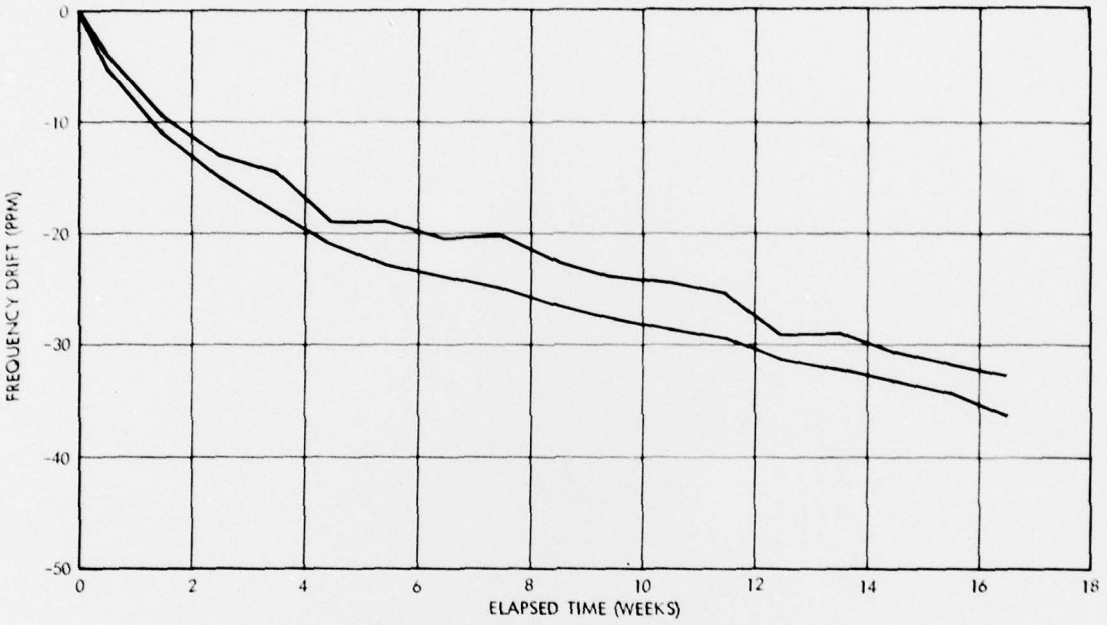

Figure 5-5. SAW Oscillator Aging for Cr/Au Metallized Delay Lines